

**NASA Contractor Report 181903**  
**ICASE Report No. 89-57**

# ICASE

## **A HIGH-ORDER LAGRANGIAN-DECOUPLING METHOD FOR THE INCOMPRESSIBLE NAVIER-STOKES EQUATIONS**

**L. Ho, Y. Maday,  
A. Patera, E. Rønquist**

Contract No. NAS1-18605  
September 1989

Institute for Computer Applications in Science and Engineering  
NASA Langley Research Center  
Hampton, Virginia 23665-5225

Operated by the Universities Space Research Association

(NASA-CR-181903) A HIGH-ORDER  
LAGRANGIAN-DECOUPLING METHOD FOR THE  
INCOMPRESSIBLE NAVIER-STOKES EQUATIONS Final  
Report (ICASE) 48 p

CSC 12A

N90-10631

Unclas

63/04 0232363



National Aeronautics and  
Space Administration

**Langley Research Center**  
Hampton, Virginia 23665-5225

Handwritten text at the top of the page, possibly a header or title, which is mostly illegible due to blurring and low contrast.

Horizontal lines of text at the bottom of the page, likely a footer or a list of items, which are also illegible.

# A HIGH-ORDER LAGRANGIAN-DECOUPLING METHOD FOR THE INCOMPRESSIBLE NAVIER-STOKES EQUATIONS

Lee-Wing Ho<sup>†</sup>, Yvon Maday<sup>†\* 1</sup>, Anthony T. Patera<sup>†</sup>, & Einar M. Rønquist<sup>†</sup>

<sup>†</sup>Department of Mechanical Engineering,  
M.I.T., Cambridge, MA 02139, U.S.A.

\* Laboratoire CNRS d'Analyse Numérique,  
Université Pierre et Marie Curie 75252,  
Paris, Cedex 05, France

## ABSTRACT

In this paper we present a high-order Lagrangian-decoupling method for the unsteady convection-diffusion and incompressible Navier-Stokes equations. The method is based upon: Lagrangian variational forms that reduce the convection-diffusion equation to a symmetric initial value problem; implicit high-order backward-differentiation finite-difference schemes for integration along characteristics; finite element or spectral element spatial discretizations; mesh-invariance procedures and high-order explicit time-stepping schemes for deducing function values at convected space-time points. The method improves upon previous finite element characteristic methods through the systematic and efficient extension to high order accuracy, and the introduction of a simple structure-preserving characteristic-foot calculation procedure which is readily implemented on modern architectures. The new method is significantly more efficient than explicit-convection schemes for the Navier-Stokes equations due to the decoupling of the convection and Stokes operators and the attendant increase in temporal stability. Numerous numerical examples are given for the convection-diffusion and Navier-Stokes equations for the particular case of a spectral element spatial discretization.

---

<sup>1</sup>This research was supported in part by the National Aeronautics and Space Administration under NASA Contract No. NAS1-18605 while the second author was in residence at the Institute for Computer Applications in Science and Engineering (ICASE), NASA Langley Research Center, Hampton, VA 23665.

## 1. Introduction

A large class of important fluid flows is described by the incompressible Navier-Stokes equations,

$$u_{m,t} + u_q u_{m,q} = -p_{,m} + \nu u_{m,qq} + f_m \quad \text{in } \Omega \quad (1a)$$

$$u_{q,q} = 0 \quad \text{in } \Omega \quad , \quad (1b)$$

where  $\underline{x} = (x_m)_{m=1,\dots,d}$  is the space variable in  $\Omega$  of  $\mathbb{R}^d$ ,  $t$  is time,  $\underline{f}(\underline{x}, t)$  is the prescribed force,  $\underline{u}(\underline{x}, t) = (u_m(\underline{x}, t))_{m=1,\dots,d}$  is the velocity,  $p(\underline{x}, t)$  is the pressure normalized by a (constant) density, and  $\nu$  is the kinematic viscosity. We adopt Cartesian tensor indicial notation, with  $u_{m,q} = \frac{\partial u_m}{\partial x_q}$ ,  $u_{m,t} = \frac{\partial u_m}{\partial t}$ , and summation over repeated subscripts,  $u_{q,q} = \sum_{q=1}^d \frac{\partial u_q}{\partial x_q}$ . Equation (1a) represents conservation of momentum for a Newtonian fluid, while equation (1b) represents conservation of mass for an essentially incompressible flow.

The difficulties associated with numerical solution of the incompressible Navier-Stokes equations arise from two distinct sources: the pressure-divergence terms, and the convection diffusion contributions. The pressure-divergence terms require first, for optimal convergence, that proper discrete function spaces be chosen for the velocity and pressure [1], and second, for rapid solution, that algorithms be developed that effectively decouple the pressure and velocity [e.g., 2-4]. The origin of the numerical difficulties associated with the convection and convection-diffusion terms are equally well documented, but less resolved: convection-diffusion introduces thin boundary layers for small  $\nu$ ; the imbalance of convection and diffusion leads to weak spatial ‘‘stability’’ for small  $\nu$ , in that the ratio of the continuity and coercivity constants becomes large [5]; timescales for equilibration become large for small  $\nu$ ; the convection term destroys the isotropy and symmetry of the Stokes operator for *all* values of  $\nu$ .

To motivate our new class of schemes we briefly summarize standard numerical approaches to the *time-dependent* Navier-Stokes equations. In particular, we note that the unsteady Navier-Stokes equations are often treated in a semi-implicit fashion, in which

the symmetric Stokes operator is handled implicitly and the convection term is treated explicitly,

$$\begin{aligned} \frac{u_m^{n+1} - u_m^n}{\Delta t} + \mathcal{F}([u_q u_{m,q}]^n, [u_q u_{m,q}]^{n-1}, \dots) = \\ - p_{,m}^{n+1} + \mathcal{G}([\nu u_{m,qq} + f_m]^{n+1}, [\nu u_{m,qq} + f_m]^n, \dots) \quad \text{in } \Omega \end{aligned} \quad (2a)$$

$$u_{q,q}^{n+1} = 0 \quad \text{in } \Omega \quad . \quad (2b)$$

Here  $\underline{u}^n(\underline{x}) = \underline{u}(\underline{x}, n\Delta t)$ , where  $\Delta t$  is the time step, and  $\mathcal{F}$  and  $\mathcal{G}$  are appropriate explicit and implicit time-marching schemes [6], respectively. Explicit treatment of the convective term is motivated by the fact that solution of the (nonlinear) implicit convection equations is difficult; no efficient (faster-than-time-like) robust *iterative* methods are available for general unsymmetric anisotropic operators, and *direct* methods are typically memory-intensive, costly, and serial, in particular in higher space dimensions. These arguments for explicit convection, although by no means universally accepted (e.g., [7]), are most easily defended for *high-order* spatial discretizations, in which asymmetry and bandwidth problems are further aggravated by longer-range coupling.

The semi-implicit method of equation (2) is intended to represent a compromise of convenience and efficiency between the symmetric Stokes operator and the unsymmetric convection term; unfortunately, it is not an optimal compromise, as we now describe. To begin, we assume that the semi-discretization (2) is further discretized in space, with the spatial discretization characterized by an effective mesh spacing  $h$ . We next (plausibly) assume that the critical time step set by the explicit convection treatment,

$$\Delta t_{cr} \sim \mathcal{O}(h/|\underline{u}|),$$

is smaller than the time step required for accuracy,  $\Delta t_{acc}$ , and that stability thus determines the timestep. The work required to integrate (2) to a final time  $T$ ,  $\mathcal{W}^{s.i.}$  (semi-implicit), is then

$$\mathcal{W}^{s.i.} = (T/\Delta t_{cr})\mathcal{W}_{\Delta t} \quad (3a)$$

where  $\mathcal{W}_{\Delta t}$  is the total work per timestep (e.g., in clock cycles). The total work per timestep  $\mathcal{W}_{\Delta t}$  is further broken up as:

$$\mathcal{W}_{\Delta t} = a\mathcal{W}_{\Delta t,c}^{eval} + \mathcal{W}_{\Delta t,s}^{inv} . \quad (3b)$$

Here the convective work per timestep is given by  $\mathcal{W}_{\Delta t,c} = a\mathcal{W}_{\Delta t,c}^{eval}$ , where  $\mathcal{W}_{\Delta t,c}^{eval}$  is the work required to *evaluate* the convective terms, and  $a$  is the (order unity) number of evaluations required for  $\mathcal{F}$ , and the Stokes work per timestep,  $\mathcal{W}_{\Delta t,s}$ , is equal to the work required to *invert* the Stokes system,  $\mathcal{W}_{\Delta t,s}^{inv}$ .

Finally, we note that for nontrivial problems it is typically the case that  $\mathcal{W}_{\Delta t,c}^{eval} \ll \mathcal{W}_{\Delta t,s}^{inv}$ , as the solution for the pressure in incompressible simulations requires *at least* an elliptic solve [8-10], and, more properly, nested elliptic solves [2-4] at *each* timestep. For instance, for typical spectral-element-discretization Navier-Stokes calculations,  $\mathcal{W}_{\Delta t,c}^{eval}$  is an order of magnitude less than  $\mathcal{W}_{\Delta t,s}^{inv}$  for splitting Poisson schemes [11-13], and several orders-of-magnitude less than  $\mathcal{W}_{\Delta t,s}^{inv}$  for consistent Uzawa methods [4,14,15]. (Note that explicit treatment of the viscous terms does not significantly alter these estimates, as the majority of the work  $\mathcal{W}_{\Delta t,s}^{inv}$  derives directly from the elliptic pressure term.) These complexity estimates are based on relatively efficient conjugate-gradient [14] and multigrid [16,17] elliptic solvers [4,14,15], and although  $\mathcal{W}_{\Delta t,s}^{inv}$  will certainly be reduced by further improvements in elliptic technology, it is clear that  $\mathcal{W}_{\Delta t,s}^{inv}$  will always remain significantly larger than  $\mathcal{W}_{\Delta t,c}^{eval}$ .

It is now readily seen in what sense semi-implicit methods are not entirely satisfactory. The usual motivation for turning to an explicit rather than implicit formulation is that the increase in number of timesteps ( $T/\Delta t$ ) is more than counteracted by an associated decrease in work per timestep,  $\mathcal{W}_{\Delta t}$ . However, it is clear from (3) that for the Navier-Stokes equations an increase in  $T/\Delta t$  from  $T/\Delta t_{acc}$  to  $T/\Delta t_{cr}$  is *not* compensated for by a commensurate or greater decrease in  $\mathcal{W}_{\Delta t}$ , as the majority of the work per timestep is due to the *elliptic* solves,  $\mathcal{W}_{\Delta t,s} >> \mathcal{W}_{\Delta t,c}$ . A better compromise is required, in which

$T/\Delta t \ll T/\Delta t_{cr}$ , and  $\mathcal{W}_{\Delta t,c}$  and  $\mathcal{W}_{\Delta t,s}$  are of the same order; such a “balanced” scheme would clearly result in improvements in computational efficiency, in particular for high-order spatial discretizations. These comments are especially relevant when (2) is viewed a method for the solution of the steady-state equations.

We present in this paper a new high-order Lagrangian-decoupling method for the convection-diffusion and Navier-Stokes equations based on high-order finite-differences in “time” and variational (finite or spectral element) discretizations in “space”. The scheme preserves symmetry as regards the diffusion and Stokes operators, thereby allowing for fast and robust iterative solution, yet provides for much better temporal stability for the full Navier-Stokes equations than explicit-convection alternatives such as (2); in essence, the new method exchanges a significant increase in  $\Delta t$  above  $\Delta t_{cr}$  for an easily accomodated increase in the convective work that brings  $\mathcal{W}_{\Delta t,c}$  into *balance* with  $\mathcal{W}_{\Delta t,s}$ . The direct ancestors of the method are the Lagrangian and arbitrary-Lagrangian-Eulerian finite element techniques [18,19], however the technique can also be thought of as a rigorous subcycling approach [20], or as a high-order non-dissipative upwinding scheme [21,22]. The essential differences between our method and its closest predecessor, the characteristic scheme of Pironneau [18], are the systematic and efficient extension to high-order accuracy, and a simple structure-preserving Lagrangian remeshing scheme (characteristic-foot calculation) which is readily implemented on modern architectures.

The structure of the paper is as follows. In Section 2 we introduce the strong and Lagrangian variational forms of the convection-diffusion equation. In Section 3 we describe the nodal function spaces for finite [23] or spectral [14,24] element spatial discretization; we present the new high-order finite-difference-in-“time” Lagrangian-decoupling method; and we summarize the stability, accuracy, and computational complexity of the new technique. In Section 4 we briefly describe an extension of the scheme to the full unsteady nonlinear Navier-Stokes equations. Lastly, in Section 5, numerous numerical examples are given of the new scheme for the particular case of a spectral element spatial discretization.

## 2. Convection-Diffusion Equation

### 2.1 Strong Form

In this paper we shall adopt the common practice of using the convection-diffusion equation as a simple model for the Navier-Stokes equations (1). As our scheme is particularly tied to the structure of the incompressible Navier-Stokes equations (the inequality  $\mathcal{W}_{\Delta t, \epsilon} \ll \mathcal{W}_{\Delta t, \delta}$  is only occasionally true for convection-diffusion alone), it is imperative that we return to the parent equation to demonstrate that our method is, indeed, applicable to the full Navier-Stokes system. This extension is described and illustrated in Sections 4 and 5, respectively.

Our simple convection-diffusion equation is given by

$$\phi_{,t} + u_q \phi_{,q} = \nu \phi_{,qq} + g \quad \forall t \in (0, T), \quad \forall \underline{x} \in \Omega \quad , \quad (4)$$

where  $\phi(\underline{x}, t)$  is a passive scalar,  $\underline{u}$  is the prescribed convection velocity,  $\underline{x}$  is space,  $t$  is time,  $\nu$  is diffusivity,  $g(\underline{x}, t)$  is a prescribed source, and  $\Omega$  is the domain in  $\mathbb{R}^d$ . In addition to equation (4) we require initial conditions

$$\phi(\underline{x}, t = 0) = 0 \quad \forall \underline{x} \in \Omega \quad , \quad (5)$$

and boundary conditions

$$\phi(\underline{x}, t) |_{\partial\Omega} = 0 \quad \forall t \in (0, T) \quad , \quad (6)$$

where  $\partial\Omega$  denotes the boundary of  $\Omega$ , and  $\hat{n}$  will denote the unit outward normal on  $\partial\Omega$ . The simple initial conditions (5) and homogeneous essential boundary conditions (6) are chosen for clarity of presentation; the method, in fact, applies to general non-homogeneous and non-essential boundary conditions [25].

For the passive scalar equation (4) the convection velocity  $\underline{u}$  is prescribed. The field  $\underline{u}$  is required to be solenoidal,

$$u_{m,m} = 0 \quad (7)$$

to vanish on the domain boundary,

$$\underline{u} |_{\partial\Omega} = \underline{0} \quad (8)$$

and to be independent of time,

$$\underline{u} = \underline{u}(\underline{x}) \quad (9)$$

The requirement (8) is closely coupled to (6), and can be relaxed to include inflow and outflow conditions [25]. Time-dependent  $\underline{u}$  will be considered in Section 4 in the context of the Navier-Stokes equations.

## 2.2 Weak Forms

Our numerical formulation rests on two Lagrangian variational forms, the first for the convection-diffusion equation (4), the second for a seemingly trivial equation which we shall denote the “invariance” equation. To better motivate these variational forms, we remark that our numerical scheme, like previous finite-element characteristic methods [18,19], corresponds to finite-difference methods in space-time along  $\underline{u}$ -characteristics, and variational methods in space. The purpose of the Lagrangian variational forms is first, to (Lagrangian) transform “space” into “time” as regards the convection operator, and second, to allow for (variational) finite or spectral element spatial discretization of the diffusion operator.

### a. Convection-Diffusion Equation

To pose the variational problems we first define the classical Sobolev spaces  $L^2(\Omega)$  and  $H_0^1(\Omega)$  [26],

$$L^2(\Omega) = \{v(\underline{x}) \text{ measurable in } \Omega, \int_{\Omega} v^2 d\Omega < \infty\} \quad (10a)$$

$$H_0^1(\Omega) = \{v(\underline{x}) \in L^2(\Omega); v_{,q} \in L^2(\Omega), q = 1, \dots, d, v |_{\partial\Omega} = 0\} : \quad (10b)$$

In what follows we shall denote the space  $H_0^1(\Omega)$  as  $Y$ . We shall also require the temporal-spatial space  $Z$  defined by

$$Z = \left\{ v \text{ measurable in } \Omega \times (0, T), \int_0^T \int_{\Omega} (v^2 + \sum_{q=1}^d (v_{,q})^2) d\Omega dt' < \infty, \right. \\ \left. v(\underline{x}, t) \in H_0^1(\Omega) \text{ a.e. } t \in (0, T) \right\}, \quad (11)$$

where  $T$  is the final time of integration. The norms associated with these spaces will be denoted by  $\| \cdot \|_{L^2}$ ,  $\| \cdot \|_{H^1}$ , and  $\| \cdot \|_Z$ , respectively.

The Lagrangian variational form of the equations (4)-(6) is then: Find  $\phi \in Z$  such that  $\phi(\underline{x}, t = 0) = 0$ , and  $\forall t \in (0, T)$

$$\frac{d}{dt} \left\{ \int_{\Omega} \psi \phi d\Omega \right\} = -\nu \int_{\Omega} \psi_{,i} \phi_{,i} d\Omega + \int_{\Omega} \psi g d\Omega \quad (12)$$

for all  $\psi \in Z$  such that  $\hat{\psi}(\underline{x}, s = 0) = \psi_0(\underline{x})$ , and  $\forall s = T - t \in (0, T)$

$$\hat{\psi}_{,i} - u_{,q} \hat{\psi}_{,q} = 0 \quad \forall \underline{x} \in \Omega \quad (13)$$

for some  $\psi_0(\underline{x}) \in H_0^1(\Omega)$ . Here  $\hat{\psi}(\underline{x}, s) = \psi(\underline{x}, T - s)$ . Equation (12) is readily derived from the strong form (4)-(6) by integration by parts in space and time, use of "Reynolds transport theorem", and substitution of equation (13) [27]; note that the particularly simple form of the first term in equation (12) requires a solenoidal convecting velocity field  $\underline{u}$ . We now suppose that the domain  $\Omega$  is the image of some reference domain  $\bar{\Omega}$  through a smooth, invertible mapping  $\mathcal{A}: \bar{\Omega} \rightarrow \Omega$ . The equation (13) for the test function  $\hat{\psi}(\underline{x}, s)$  can then be written in Lagrangian form,

$$\begin{cases} \frac{\partial \underline{X}}{\partial s}(\underline{a}, s) = -\underline{u}(\underline{X}(\underline{a}, s)) \\ \frac{\partial}{\partial s} \hat{\psi}(\underline{X}(\underline{a}, s), s) = 0 \end{cases} \quad \forall s \in (0, T), \quad \forall \underline{a} \in \bar{\Omega} \quad (14a)$$

$$\begin{cases} \underline{X}(\underline{a}, s = 0) = \underline{x} & \forall \underline{a} \in \bar{\Omega} \\ \hat{\psi}(\underline{x}, s = 0) = \psi_0(\underline{x}) & \forall \underline{x} \in \Omega \end{cases}, \quad (14b)$$

where  $\underline{X}$  is a standard Lagrangian spatial variable. The variable  $\underline{X}$  will remain smooth for smooth  $\underline{u}$ .

Note that equations (12) and (14) are the variational restatement of the simple physical fact that the rate of change of  $\phi$  in space-time along a characteristic of the convection equation is equal to the divergence of the diffusion fluxes. In our numerical scheme the convection initial value problem will be treated by high-order finite-differences, and the diffusion boundary value problem will be treated by finite or spectral elements.

## b. Invariance Equation

As with all Lagrangian schemes, some form of remeshing or characteristic-foot calculation is required for the scheme to proceed for long times. A key element of our high-order scheme is a remeshing strategy which is both efficient and accurate; the method is based on an invariance procedure, in which we associate to any continuous function  $\bar{q}(\underline{x}) \in H_0^1(\Omega)$  a new function  $q(\underline{x}, s)$  and related (trivial) evolution equation

$$q(\underline{x}, s = 0) = \bar{q}(\underline{x}), \quad \frac{\partial}{\partial s} q(\underline{x}, s) = 0 \quad \forall \underline{x} \in \Omega \quad . \quad (15)$$

Equation (15) can be written in a  $\underline{u}$ -Lagrangian variational form as: Find  $q(\underline{x}, s) \in Z$  such that  $q(\underline{x}, s = 0) = \bar{q}(\underline{x})$ , and  $\forall s \in (0, S)$

$$\frac{d}{ds} \left\{ \int_{\Omega} pq \right\} + \int_{\Omega} pu_m q_{,m} = 0 \quad (16)$$

for all  $p \in Z$  such that  $p(\underline{x}, s = 0) = p_0(\underline{x})$ , and  $\forall s \in (0, S)$

$$p_{,s} - u_m p_{,m} = 0 \quad \forall \underline{x} \in \Omega \quad (17)$$

for some  $p_0(\underline{x}) \in H_0^1(\Omega)$ . Equation (17) for  $p(\underline{x}, s)$  can be written in Lagrangian form,

$$\begin{cases} \frac{\partial \underline{X}}{\partial s}(\underline{a}, s) = -\underline{u}(\underline{X}(\underline{a}, s)) \\ \frac{\partial}{\partial s} p(\underline{X}(\underline{a}, s), s) = 0 \end{cases} \quad \forall s \in (0, S), \quad \forall \underline{a} \in \tilde{\Omega} \quad (18a)$$

$$\begin{cases} \underline{X}(\underline{a}, s = 0) = \underline{x} \\ p(\underline{x}, s = 0) = p_0(\underline{x}) \end{cases} \quad \begin{matrix} \forall \underline{a} \in \tilde{\Omega} \\ \forall \underline{x} \in \Omega \end{matrix} \quad , \quad (18b)$$

with  $\tilde{\Omega}$  defined as for equation (14).

The equivalence of ((16), (18)) and (15) can be understood by noting that the  $\underline{u}$ -motion of the “mesh” through (18) is *cancelled* in (16) by the  $\underline{u}$ -convection term. Although it may appear overly complicated to re-introduce Lagrangian convection by the  $\underline{u}$ -field into an equation (15) which is essentially Eulerian, this will allow us to accurately remesh variables while preserving the underlying structure of the spatial discretization. Indeed, we shall see that the Lagrangian simplification of (4) in (12) in exchange for the Lagrangian complication of (15) in (16) is equivalent to striking a better balance between  $\Delta t$  and  $W_{\Delta t, c}/W_{\Delta t, s}$ .

Remark on Inflow/Outflow Boundary Conditions: We note that although we have implicitly written the hyperbolic equation (16) as having Dirichlet boundary conditions on  $\partial\Omega$  (i.e.,  $q(\underline{x}, s) \in Z$ ), this is, in fact, equivalent to the proper choice of *no* boundary conditions (recall  $u_m \hat{n}_m = 0$ ), given that  $\bar{q}(\underline{x}) \in H_0^1$ . In treating inflow/outflow problems (in which we impose essential boundary conditions on  $\phi$  at inflow,  $u_m \hat{n}_m < 0$ , and natural boundary conditions on  $\phi$  at outflow,  $u_m \hat{n}_m > 0$ ), we require boundary conditions on  $q$  in (16) *only* at inflow, with this inflow value obtained through extension of the inflow profile upstream.

### 3. Discrete Equations

#### 3.1 Spatial Discretization

##### a. Discrete Function Spaces

We first need to generate the discrete function spaces (“nodal finite element spaces”) associated with the space  $Y = H_0^1(\Omega)$ , after which our method will follow directly from the Lagrangian variational forms of Section 2.2 and high-order finite-difference discretization of the “time” terms in equation (12) and (16). We begin by assuming a conforming, non-overlapping domain decomposition [28]  $\mathcal{D}$ ,

$$\bar{\Omega} = \bigcup_{k=1}^K \bar{\Omega}^k, \quad (19)$$

in which the  $\Omega^k$  are defined with respect to reference volumes  $\hat{\Omega}^k$  (e.g., a segment in  $\mathbb{R}^1$ , a triangle or square in  $\mathbb{R}^2$ , a tetrahedron or cube in  $\mathbb{R}^3$ ) by an invertible elemental mapping (in fact,  $\mathcal{A}$  of equation (14)),

$$\underline{\xi} \in \hat{\Omega}^k \xrightarrow{F_m^{i,k}(\underline{\xi})} x_m \in \Omega^k \quad \forall m \in \{1, \dots, d\} \quad (20a)$$

$$\underline{x} \in \Omega^k \xrightarrow{F_m^{-1,i,k}(\underline{x})} \xi_m \in \hat{\Omega}^k \quad \forall m \in \{1, \dots, d\}. \quad (20b)$$

The decomposition is *geometrically* conforming in that we require that the intersection  $\Gamma = \partial\Omega^k \cap \partial\Omega^l$  be either null, or an entire face, edge, or vertex of both  $\Omega^k$  and  $\Omega^l$ .

Within each reference domain  $\hat{\Omega}^k, k = \{1, \dots, K\}$ , we introduce a polynomial space  $\mathbb{P}^k(\hat{\Omega}^k)$ , a unisolvent set of  $N^k$  basis points  $\xi_m^{i,k}, m \in \{1, \dots, d\}, i \in \{1, \dots, N^k\}$ , and a set of associated Lagrangian interpolants  $Q^{i,k}$ ,

$$\begin{aligned} Q^{i,k} &\in \mathbb{P}^k(\hat{\Omega}^k) \\ Q^{i,k}(\underline{\xi}^{j,k}) &= \delta_{ij} \quad \forall i, j \in \{1, \dots, N^k\}^2, \end{aligned} \quad (21)$$

where  $\delta_{ij}$  is the Kronecker delta symbol. For *functional* conformity we require that the  $IP^k(\hat{\Omega}^k)$  and  $\underline{F}^{\cdot,k}$  be chosen such that for all  $k \in \{1, \dots, K\}$  and for any  $v(\underline{\xi}) \in IP^k(\hat{\Omega}^k)$  and any  $\underline{x} \in \Gamma = \partial\Omega^k \cap \partial\Omega^l$  such that  $\Gamma$  is non-null there exists a  $w \in IP^l(\hat{\Omega}^l)$  such that  $w(\underline{F}^{-1,l}(\underline{x})) = v(\underline{F}^{-1,k}(\underline{x}))$ . With our nodal Lagrangian-interpolant representation we now make precise the particular *isoparametric* map  $F_m^{\cdot,k}$  of interest in our Lagrangian characteristic technique,

$$F_m^{\cdot,k}(\underline{\xi}) = \sum_{i=1}^{N^k} X_m^{i,k} Q^{i,k}(\underline{\xi}) \quad \forall m \in \{1, \dots, d\} \quad \forall k \in \{1, \dots, K\}, \quad (22)$$

in which the  $\underline{X}^{i,k}$  are the images of the  $\underline{\xi}^{i,k}$ .

In addition to the conforming assumption on the  $IP^k(\hat{\Omega}^k)$  and  $\underline{F}^{\cdot,k}$  we require: the  $\underline{\xi}^{i,k}$  be chosen such that those  $\underline{\xi}^{i,k}$  on  $\partial\Omega^k$  are unisolvent with respect to the trace space of  $IP^k(\hat{\Omega}^k)$ ; the usual “local-global” coincidence condition on the  $\underline{X}^{i,k}$  (e.g., for each  $\underline{\xi}^{i,k}$  on an edge shared by elements  $k$  and  $l$ , there must exist a unique  $\underline{\xi}^{j,l}$  which maps to the same global point),

$$\underline{X}^{j,k} = \underline{X}^i \quad \forall i \in \{1, \dots, \mathcal{N}\}, \quad \forall (j,k) \in \mathcal{S}_i. \quad (23)$$

Here  $\mathcal{N}$  is the number of global nodes in the system, and  $\mathcal{S}_i$  is the set of (local node, element) couples associated with the unique global node  $\underline{X}^i$ . Note that although we introduce here the standard finite element global identifier  $\mathcal{S}_i$  to describe inter-element connectivity and continuity, this construct serves purely for purposes of succinct presentation; in practice, our schemes are based entirely on element-local constructs (see Section 5) [13,14,29]. Summarizing our superscript notation:  $X$  refers to a globally defined quantity;  $X^{\cdot,k}$  to an elementally defined quantity;  $X^{i,k}$  to a nodally/elementally defined quantity; and  $X^i$  to a nodally/globally defined quantity.

We can now define our discrete polynomial subspace  $Y_h(\underline{X}^i) \subset H_0^1(\Omega) = Y$  as

$$Y_h(\underline{X}^i) = \text{span} \left( \sum_{(j,k) \in \mathcal{S}_i} \bar{Q}^{j,k}(\underline{x}) \quad \forall i \in \{1, \dots, \mathcal{N}\}_{/E} \right) \quad (24a)$$

where  $\forall k \in \{1, \dots, K\}$  and  $\forall j \in \{1, \dots, N^k\}$

$$\bar{Q}^{j,k}(\underline{x}) = \begin{cases} Q^{j,k}(F^{-1},k(\underline{x})) & \forall \underline{x} \in \bar{\Omega}^k \\ 0 & \forall \underline{x} \notin \bar{\Omega}^k \end{cases}, \quad (24b)$$

where the set  $\{1, \dots, \mathcal{N}\}'_{/B}$  excludes those  $i \in \{1, \dots, \mathcal{N}\}$  for which  $\underline{X}^i$  is on  $\partial\Omega$ . The space  $Y_h(\underline{X}^i)$  is thus characterized by the domain decomposition  $\mathcal{D}$ , by  $h$ , symbolic for the  $IP^k(\hat{\Omega}^k)$ ,  $k = 1, \dots, K$ , and by the the global nodes  $\underline{X}^i$ . The basis we choose to *represent*  $v_h \in Y_h$  is the nodal basis used to *describe* the space in (24)

$$v_h(\underline{x}) = \sum_{i=1}^{\mathcal{N}} v_h^i \sum_{(j,k) \in \mathcal{S}_i} \bar{Q}^{j,k}(\underline{x}) \quad (25a)$$

$$v_h^i = 0 \quad i \in \{1, \dots, \mathcal{N}\}'_{/B}, \quad (25b)$$

where the set  $\{1, \dots, \mathcal{N}\}'_{/B}$  is the complement of  $\{1, \dots, \mathcal{N}\}'_{/B}$  in  $\{1, \dots, \mathcal{N}\}$ , and  $v_h^i = v_h(\underline{X}^i)$ . For simplicity we shall write  $v_h^i = v^i$ , and explicitly write  $q(\underline{X}^i)$  to denote the nodal values of a function  $q$  not *a priori* in  $Y_h(\underline{X}^i)$ .

## b. Discrete Inner Products

Having defined our spaces in Section 3.1a, we now complete the spatial discretization by defining the discrete inner products associated with the continuous inner products required in the variational forms defined in 2.2. To begin, we remark that the convection-diffusion equation (12) requires two inner products, the  $L^2$  inner product and an  $H^1$  bilinear form. Their discrete forms with respect to our space  $Y_h$  are

$$\begin{aligned} \forall \psi^i, \phi^j \in (\mathbb{R}^{\mathcal{N}})^2 \quad & \sum_{i=1}^{\mathcal{N}} \sum_{j=1}^{\mathcal{N}} \psi^i B^{ij}(\underline{X}^i) \phi^j \equiv \\ & \sum_{i=1}^{\mathcal{N}} \sum_{j=1}^{\mathcal{N}} \psi^i \phi^j \sum_{\substack{p,q,k \dots i. \\ (p,k) \in \mathcal{S}_i \\ (q,k) \in \mathcal{S}_j}} \int_{\Omega^k} Q^{p,k}(\underline{\xi}) Q^{q,k}(\underline{\xi}) J^{i,k}(\underline{\xi}) d\underline{\xi} \quad , \end{aligned} \quad (26)$$

and

$$\forall \psi^i, \phi^j \in (\mathbb{R}^{\mathcal{N}})^2 \quad \sum_{i=1}^{\mathcal{N}} \sum_{j=1}^{\mathcal{N}} \psi^i A^{ij}(\underline{X}^i) \phi^j \equiv$$

$$\sum_{i=1}^{\mathcal{N}} \sum_{j=1}^{\mathcal{N}} \psi^i \phi^j \sum_{\substack{p,q,k \dots i. \\ (p,k) \in \mathcal{S}_i \\ (q,k) \in \mathcal{S}_j}} \int_{\Omega^h} G_{m,n}^{i,k} Q_{,n}^{p,k} G_{m,n}^{j,k} Q_{,n}^{q,k} (J^{i,k})^{-1} d\underline{\xi} \quad , \quad (27)$$

respectively. Here  $J^{i,k}(\underline{\xi})$  and  $G_{m,n}^{i,k}(\underline{\xi})$  are the Jacobian and the derivative transformation matrix associated with the change of variables (22),

$$J^{i,k}(\underline{\xi}) = \det F_{m,q}^{i,k}(\underline{\xi}) \quad (28a)$$

and

$$G_{m,p}^{i,k}(\underline{\xi})(J^{i,k})^{-1} F_{p,q}^{i,k}(\underline{\xi}) = \delta_{m,q} \quad , \quad (28b)$$

respectively. The invariance equation (16) requires the  $L^2$  inner product (26), as well as a convection operator,

$$\begin{aligned} \forall \psi^i, \phi^j \in (\mathbb{R}^{\mathcal{N}})^2 \quad & \sum_{i=1}^{\mathcal{N}} \sum_{j=1}^{\mathcal{N}} \psi^i D^{ij}(\underline{X}^i) \phi^j \equiv \\ & \sum_{i=1}^{\mathcal{N}} \sum_{j=1}^{\mathcal{N}} \psi^i \phi^j \sum_{\substack{p,q,k \dots i. \\ (p,k) \in \mathcal{S}_i \\ (q,k) \in \mathcal{S}_j}} \int_{\Omega^h} u_m Q^{p,k} G_{m,n}^{i,k} Q_{,n}^{q,k} d\underline{\xi} \quad . \end{aligned} \quad (29)$$

In (26)-(28)  $\int$  refers either to exact quadrature or numerical quadrature, depending on the particular spatial discretization chosen (see Section 5).

Lastly, we require the linear form

$$\begin{aligned} \forall \psi^i \in \mathbb{R}^{\mathcal{N}} \quad & \sum_{i=1}^{\mathcal{N}} \psi^i \ell^i(\underline{X}^i) g \equiv \\ & \sum_{i=1}^{\mathcal{N}} \psi^i \sum_{(p,k) \in \mathcal{S}_i} \int_{\Omega^h} Q^{p,k}(\underline{\xi}) q_{\Omega^h}(\underline{F}^{i,k}(\underline{\xi})) J^{i,k}(\underline{\xi}) d\underline{\xi} \quad , \end{aligned} \quad (30)$$

for the inhomogeneous term in (12).

### 3.2 Full Discretization

Our fully discrete convection-diffusion equation now corresponds to insertion of the discrete linear and bilinear forms of (26)-(30) into the variational form (12), followed by

discretization of the “space-time” derivative associated with the left-hand side of (12) by the  $Q$ th order backward-differentiation implicit finite-difference formula [6]: Find  $\bar{\phi}^{j;n+1} = \phi^{j;n+1} = \phi^j(t^{n+1} = (n+1)\Delta t)$  such that

$$\sum_{j=1}^{\mathcal{N}} \sum_{q=0}^Q \beta_q B^{ij}(\underline{X}^{l;n+1-q}) \bar{\phi}^{j;n+1-q} = \beta^i \left\{ \sum_{j=1}^{\mathcal{N}} A^{ij}(\underline{X}^{l;n+1}) \phi^{j;n+1} + \ell^i(\underline{X}^{l;n+1}) g^{i;n+1} \right\}, \quad \forall i \in \{1, \dots, \mathcal{N}\}'_{\mathcal{B}} \quad (31a)$$

$$\bar{\phi}^{i;n+1} = 0 \quad \forall i \in \{1, \dots, \mathcal{N}\}'_{\mathcal{B}} \quad (31b)$$

Here  $\underline{X}^{l;n+1} \equiv \underline{X}^{l;*$  refers to the the base (“undeformed”) discretization of  $\Omega$ , and thus the  $A^{ij}(\underline{X}^{l;n+1}), \ell^i(\underline{X}^{l;n+1})$  are *known*; it can also be shown from the incompressibility of  $\underline{u}$  and (14a) that  $B^{ij}(\underline{X}^{l;n+1-q})$  is, in fact, independent of  $\underline{X}^l$ , and can thus be taken as  $B^{ij}(\underline{X}^{l;n+1})$ . Note that any nodal variable *without* tilde refers to nodal values at the base-discretization points  $\underline{X}^{l;*$ . The backward differentiation coefficients are given in [6] with  $\beta_q \sim \mathcal{O}(1/\Delta t)$ , and  $\beta^i \sim \mathcal{O}(1)$ .

It remains now to find the  $\bar{\phi}^{j;n+1-q}$  for  $q > 0$ ;  $\bar{\phi}^{j;n+1-q}$  represents the value of  $\phi$  at time  $t^{n+1-q}$  at the “foot” of the characteristic whose “head” at time  $t^{n+1}$  is at  $\underline{X}^{j;*$  [18]. To this end, we use our invariance procedure (16)-(18) to determine  $\bar{\phi}^{j;n+1-q}$  from the values  $\phi^{j;n+1-q}$ , the latter being *known* from previous timesteps. To wit, at each timestep  $t^{n+1}$  we perform the following subproblem:  $\forall q \in \{1, \dots, Q\}$

$$\left. \begin{aligned} \bar{\phi}^{i;n+1-q;m=0} &= \phi^{i;n+1-q} \\ \bar{\underline{u}}^{i;n+1-q;m=0} &= \underline{u}(\underline{X}^{i;*}) \\ \bar{\underline{X}}^{i;n+1-q;m=0} &= \underline{X}^{i;*} \end{aligned} \right\} \quad \forall i \in \{1, \dots, \mathcal{N}\} \quad (32)$$

$$\forall m = 0, \dots, q\Delta t/\Delta s - 1, \forall i \in \{1, \dots, \mathcal{N}\}$$

$$\begin{aligned} \frac{1}{\Delta s} \left( \sum_{j=0}^{\mathcal{N}} B^{ij}(\underline{X}^{l;im+1}) \bar{\phi}^{j;n+1-q;im+1} - \sum_{j=0}^{\mathcal{N}} B^{ij}(\underline{X}^{l;im}) \bar{\phi}^{j;n+1-q;im} \right) = \\ - \sum_{p=0}^2 \sum_{j=1}^{\mathcal{N}} \gamma_p \mathcal{D}^{ij}(\underline{X}^{l;im-p}) \bar{\phi}^{j;n+1-q;im-p} \end{aligned} \quad (33a)$$

$$\begin{aligned} \frac{1}{\Delta s} \left( \sum_{j=0}^{\mathcal{N}} B^{ij}(\underline{X}^{l;im+1}) \bar{u}^{j;im+1} - \sum_{j=0}^{\mathcal{N}} B^{ij}(\underline{X}^{l;im}) \bar{u}^{j;im} \right) = \\ - \sum_{p=0}^2 \sum_{j=1}^{\mathcal{N}} \gamma_p \mathcal{D}^{ij}(\underline{X}^{l;im-p}) \bar{u}^{j;im-p} \end{aligned} \quad (33b)$$

$$(\underline{X}^{i;im+1} - \underline{X}^{i;im})/\Delta s = - \sum_{p=0}^2 \gamma_p \bar{u}^{i;im-p}, \quad (33c)$$

$$\bar{\phi}^{i;n+1-q} = \bar{\phi}^{i;n+1-q;g \frac{\Delta t}{\Delta s}} \quad (34)$$

We have introduced here an explicit third order Adams-Bashforth scheme in  $s$  (with coefficients  $\gamma_p$  [6]) to solve the invariance problem. The subproblem timestep is  $\Delta s < \Delta t$ , with  $\frac{\Delta t}{\Delta s}$  assumed integer; the notation  $\phi^{j;n}$  refers to timestep  $n$ , while  $\bar{\phi}^{j;n;im}$  refers to *sub-timestep*  $m$  for a given  $t^n$ . Equations (33a) and (33c) correspond to discretization of (16) and (18) respectively; in conjunction with (34), (33a) and (33c) represent the Lagrangian requirement (14). Determination of the  $\bar{\phi}$  requires application of invariance to the velocity as well, (33b), as the velocity enters into the convective operator  $\mathcal{D}^{ij}$ , (29), as well as the mesh update equation for  $\underline{X}^l$ . Note that, in practice, we do not assume  $B^{ij}(\underline{X}^{l;im}) = B^{ij}(\underline{X}^{l;i^*})$  in (33a) and (33b), as actually calculating  $B^{ij}(\underline{X}^{l;im})$  from (26) appears to improve stability.

The complete scheme comprises: Lagrangian variational forms that reduce the convection-diffusion equation to a symmetric initial value problem along characteristics; high-order, *implicit* finite-difference schemes for integration along characteristics; standard

finite-element-like discretizations for the symmetric boundary-value-problem spatial operators; mesh invariance and high-order (explicit) time-stepping for deducing the function values at previous space-time points. We now turn to a summary of the characteristics of the method; the next section is a heuristic anticipation of the numerical experiments of Section 5, and of theoretical analyses treated in [25].

### 3.3 Stability, Accuracy and Computational Complexity

#### a. Stability

For the backward-differentiation scheme (31) unconditional absolute stability can be intuited in several ways. First, for the  $Q = 1$  scheme, energy arguments are readily constructed [18]. Second, for any  $Q \leq 6$  the region of absolute stability in the complex  $\lambda\Delta t$  plane for the model problem  $u_t = \lambda u$  for the backward differentiation formula includes the entire negative real axis, implying that for diffusion partial differential equations these schemes are absolutely stable. As (31) is a diffusion equation along characteristics, we expect *unconditional* stability. Indeed, it is readily shown from von-Neumann analysis that for the simple case of Fourier spatial discretization the modulus of the backwards differentiation “temporal” growth factors for *space-time* integration of convection diffusion are identical to those for *time* integration of standard diffusion; as expected, convection effects only the phase of the propagator.

As regards the application of the third order Adams Bashforth technique to the invariance equations, (33), it is clear that the usual Courant condition will apply, giving a condition of the form  $\Delta s < \mathcal{O}(h/|\underline{u}|)$ . We note that our Lagrangian-decoupling method bears a resemblance to earlier subcycle proposals [20]; an essential difference is that (33) rigorously and stably decouples the convection and elliptic (or Stokes) contributions, whereas subcycle approaches involve repeated application of the convection operator in splitting fashion.

## b. Accuracy

Convergence of  $\phi_h$  to  $\phi$  in  $H^1$  at a fixed time  $T$  (or in the  $Z$  norm) is achieved as  $\Delta t \rightarrow 0$  in (31),  $\Delta s \rightarrow 0$  in (33), and as  $Y_h \rightarrow Y$ . The error due to *space-time* integration by the backward differentiation formula in (31) is expected to be of order  $(\Delta t)^q$ . The ability to obtain virtually arbitrary-order accuracy constitutes a major difference between the current technique and past methods [18]; high-order Adams-Moulton schemes would not be stable, and would also require multiple Laplacian evaluations on deformed (not  $\underline{X}^{i*}$ ) domains. As concerns the temporal accuracy of the Adams-Bashforth treatment of the *invariance equation*, (33), we expect  $\mathcal{O}((\Delta s)^3)$  errors. The fact that the error can be controlled through  $\Delta s$  and a high-order time-stepping scheme represents a significant improvement over earlier remeshing schemes which are typically  $\mathcal{O}(\Delta t)$  [19]; low-order remeshing methods can result in strongly accuracy-limited timesteps.

The *spatial* errors are proportional to the error in the best-fit approximation of the solution  $\phi$  by the underlying discrete space  $Y_h$  [14,18,25]. In particular, for  $h$ -type finite element refinement [23] ( $K \rightarrow \infty$ ,  $N^k$  fixed) we expect algebraic convergence, and for  $p$ -type [30,31], or spectral element refinement [14,15,32] ( $K$  fixed,  $N^k \rightarrow \infty$ ) we expect spectral convergence (e.g., exponential convergence for infinitely smooth functions). Note that the spatial discretization does not only effect the treatment of the diffusion operator in (31): spatial discretization controls the numerical diffusion and dispersion in the invariance procedure (33); the allowable  $\Delta t$  in (31) is (accuracy, not stability) limited by the degree of geometric distortion that can be represented by the spatial approximation [25,33].

Since the characteristic procedure transforms space into time in the convection operator, a “time”-stepping scheme for (31) limited to low-order approximation would potentially preclude the use of a high-order method in the remaining spatial operators. The fact that the current scheme is high-order in time allows methods that are high-order in space to once again be considered in a characteristic framework. Although it might appear

that a variational (e.g., spectral) method in space would suggest a matching variational (spectral) approximation in time [24], the initial-value-problem nature of the convection operator indicates that finite-difference approximation will be more efficient, with none of the attendant "complex geometry" objections typically raised as regards high-order finite-difference approximations in space.

Lastly, it should be remarked that even the low-order ( $Q = 1$ ) scheme can be quite accurate. In particular, we note that if the invariance procedure is exact (e.g.,  $\Delta s$  small), then the temporal error in (31) is due solely to inexact integration of the diffusion terms along a characteristic. This contrasts sharply with conventional upwinding schemes [21], in which the majority of the numerical diffusion derives from mesh-induced inaccurate representation of the characteristic foot. As a result, low-order forms of (31)-(34) can achieve high accuracy if: gradients in  $\phi$  are small, and the diffusivity  $\nu$  is *small*; gradients in  $\phi$  are primarily in the cross-stream direction, that is, orthogonal to  $\underline{u}$  [5]; gradients in  $\phi$  are large in the flow direction, but the flow velocity (and hence effective spatial increment  $\Delta x = |\underline{u}| \Delta t$ ) is "small" (such as in stagnation-flow boundary layers).

### c. Computational Complexity and Generality

The beauty of the characteristic scheme [18] is that it reduces each timestep to a symmetric elliptic solve (in the case of Navier-Stokes, a symmetric Stokes solve) that can be very rapidly solved iteratively [4,14,16,17]; that is, the asymmetrizing *and* destabilizing effect of the convection operator is eliminated. For our particular implementation, the price to be paid is the solution of a "bare" (non-pressure-corrected) convection operator (33). The key to the computational efficiency of the scheme, as described in detail in equation (3) of the Introduction, is that the increase in work associated with (33),  $W_{\Delta t,c}$ , is more than compensated for by the large  $\Delta t$  allowed in (31). In particular, we note that the work

for the characteristic scheme,  $\mathcal{W}^{ch}$ , is given by

$$\mathcal{W}^{ch} = \frac{T}{\Delta t_{cr}} a' \mathcal{W}_{\Delta t, c}^{u, ai} + \frac{T}{\Delta t'_{acc}} \mathcal{W}_{\Delta t, s}^{inv} \quad , \quad (35)$$

where the first term represents (33), and the second term (31). Here  $\Delta t_{cr}$  is as in (3),  $a'$  is inflated from (3) by virtue of the additional work associated with  $Q > 1$  in (33), and  $\Delta t'_{acc}$  is the new accuracy limit that reflects the effect of geometric distortion and the accuracy of the  $Q^{th}$  order backward differentiation scheme. Although many factors must be considered to determine whether, at *fixed accuracy*,  $\mathcal{W}^{ch}$  is much less than  $\mathcal{W}^{ci}$ , the potential clearly exists for great savings. In particular, the two terms in (35) are better balanced than in (3), and the dominant work per timestep,  $\mathcal{W}_{\Delta t}$ , is effected much less frequently,  $T/\Delta t'_{acc} \ll T/\Delta t_{cr}$ . In summary, the stability-limiting and work intensive parts of the calculation have been *Lagrangian-decoupled*.

A central aspect of the efficiency of the method is the invariance procedure. Previously proposed schemes are low-order [18,19], or use a nonlinear search and solution algorithm to find the  $\phi$  directly. In the latter approach, [(33a), (33b)] are replaced by a "nonlinear solver" to obtain the  $\phi$  directly from the  $\underline{X}^i$  given by (33c) [18]. Although the "nonlinear solver" may appear faster than the time-stepping approach (33), in practice the opposite will typically be true: first, even for low-order approximations, the "nonlinear solver" approach requires non-elemental, unstructured calculations, leading to inefficient vectorization and parallelization - the time-evolution solver preserves topology and structure; second, as the "nonlinear solver" approach destroys discretization structure, tensor product representations will not be preserved, leading to orders-of-magnitude increases in work for high-order approximations ([14,34], see Section 5) - the time-evolution solver maintains an initially tensor-product representation for all "time" s.

Lastly, we briefly comment on generality. Iterative solvers, unlike direct solvers, are typically non-robust with respect to modifications to the equations and physics, as their convergence (rate) is dependent not only on discrete-equation structure, but also on the

structure of the spectrum. It is usually the case, however, that increased physical complexity in incompressible continua enters into the "divergence of the flux tensor" portion of the equation, not the acceleration term, and thus the Lagrangian-decoupling method should be *generally* applicable to a large class of problems.

#### 4. Navier-Stokes Equations

In this section we describe the extension of the convection-diffusion scheme of Section 3 to the full nonlinear unsteady Navier-Stokes equations (1). There are many ways in which to deal with the nonlinearity; we propose here a linearization technique which is both simple to implement and illustrative of the general procedure.

To begin, we consider a semi-discretization in time, in which  $u_m^{n'}(\underline{x}) = u_m(\underline{x}, n' \Delta t)$  are known for  $0 \leq n' \leq n$ , with  $u_{m,m}^{n'} = 0 \forall n' \in \{0, \dots, n\}$ . To advance the solution, that is, find  $u_m^{n+1}(\underline{x})$ , we write  $u_m(\underline{x}, t) = u_m^n(\underline{x}) + \delta u_m(\underline{x}, t)$ , and choose the *particular* linearization of (1) that yields

$$u_{m,t} + u_q^n u_{m,q} = -p_{,m} + \nu u_{m,qq} + f_m \quad \text{in } \Omega \quad (36a)$$

$$u_{q,q} = 0 \quad \text{in } \Omega \quad (36b)$$

for  $t$  near  $t^n$ . The linearization (36) is preferable over other possible distributions of  $\delta u_m$  in that stability is readily shown,  $\frac{\partial}{\partial t} \int_{\Omega} u_m u_m \leq 0$ . We now apply our Lagrangian-decoupling method and variational spatial operators exactly as for convection-diffusion, except that now the velocity appearing in the convection operator  $D^{ij}$  is frozen at  $\underline{u}^n$  during the substep (32)-(34), and the Laplacian operator in (31) is replaced with an appropriate symmetric Stokes discretization [14,15]. Note that, unlike the compressible flow case, (33a) has only a single "characteristic" direction,  $\underline{u}$ , shared by all components of the velocity.

As regards the accuracy of the resulting scheme, it is clear that the method (36) is  $\mathcal{O}(\Delta t)$  in time due to the linearization in  $\delta u_m$ ; this does not, however, preclude use of a  $\mathcal{O}((\Delta t)^q)$  scheme in space-time in the Lagrangian-decoupling procedure. In essence, the former relates to the temporal accuracy of the integration along the characteristic, whereas the latter relates to the spatial accuracy of the integration; note that when a steady-state is achieved, the  $\mathcal{O}(\Delta t)$  errors vanish, whereas the spatial errors remain. For time dependent problems, variants of (36) which are more accurate in time are readily

generated by appropriate high-order linearizations [25]. The spatial errors due to the Stokes discretization are standard [1,14,35,36], and will not be discussed further.

## 5. Spectral Element Implementation

In this section we consider the spectral element method as a particular example of the general variational spatial discretization described in Section 3.1. We give numerical results which demonstrate the convergence rate of the spectral-element-based Lagrangian-decoupling method for the convection-diffusion of a passive scalar. We also demonstrate the viability of the method for the full Navier-Stokes equations, in particular as regards increased stability and associated computational savings.

### 5.1 Description of Spectral Element Spatial Discretization

The spectral element method is a high-order variational method for the spatial discretization of partial differential equations [14,15,32]. As in (19), the computational domain is first broken up into  $K$  subdomains (spectral elements)  $\Omega^k, k = \{1, \dots, K\}$ . For reasons of efficiency (i.e., the availability of tensor product sum factorization [34]) the elements  $\Omega^k$  are taken to be line segments in  $\mathbb{R}^1$ , quadrilaterals in  $\mathbb{R}^2$ , and hexahedra (bricks) in  $\mathbb{R}^3$ , defined with respect to the reference volumes  $\hat{\Omega}^k = ]-1, 1[^d$  in  $\mathbb{R}^d$  by an invertible mapping  $F^{\cdot,k}$  (20). Although geometrically nonconforming spectral element methods have been developed [37,38], we restrict ourselves here to the conforming case.

Within each reference volume  $\hat{\Omega}^k$  the discrete polynomial subspace  $IP^k$  is taken to be the set of all polynomials of degree  $\leq N$  in each spatial direction [14]; the spectral element spatial discretization can be characterized by the discretization pair  $h = (K, N)$ . Although the particular choice of basis points  $\underline{\xi}^{i,k}$  does not effect the error estimates, it greatly effects the conditioning and sparsity of the resulting set of algebraic equations, and is critical for the efficiency of parallel iterative solution procedures [13,29]. In order to take advantage of efficient sum-factorization techniques [34], the  $N^k = (N + 1)^d$  basis points  $\underline{\xi}^{i,k}$  for  $IP^k$  are taken to be the  $d$ -tensor product of the  $N + 1$  Gauss-Lobatto Legendre points [39]; the corresponding Lagrangian interpolants  $Q^{i,k}$  of (21) are therefore the product of  $d$   $N^{i,k}$

order one-dimensional Lagrangian interpolants [14].

In the spectral element method the discrete inner products defined in Section 3.1b are based on tensor-product Gauss-Lobatto Legendre integration, that is,  $\mathfrak{I}$  is equivalent to Gaussian quadrature. The quadrature points are the same as the basis points; with  $N + 1$  quadrature points we can integrate exactly polynomials of degree  $\leq 2N - 1$ . This particular choice of numerical integration (denoted “consistent” integration) can be shown to be sufficient and optimal for most problems [14,33]. In particular, consistent integration is sufficient for complex geometries, an important consideration when considering the invariance equation (32), in which the base geometry may deform significantly.

The spectral element method combines the geometric flexibility of a low-order method with the rapid convergence rate associated with spectral techniques. Considering only spatial errors, it can be shown that the spectral element solution to the convection-diffusion equation (4) or to the full Navier-Stokes equations (1) converges spectrally fast to the exact solution for  $K$  fixed,  $N \rightarrow \infty$ , with exponential convergence obtaining for locally analytic geometry, data and solution. This rapid convergence rate derives from the good stability and approximation properties of the polynomial spaces  $P^k$ , and the accuracy associated with Gauss-Lobatto Legendre quadrature and interpolation [14,39]. Moreover, the discrete solution suffers from minimal numerical dispersion and diffusion, a fact which is important in the solution of the invariance equation (16).

Having defined our spectral element spatial discretization, we need to solve the set of algebraic equations (31)-(34) corresponding to the convection-diffusion of a passive scalar. For the implicitly treated symmetric positive-definite elliptic kernel (diffusion) in (31) we employ preconditioned conjugate gradient iteration or rapidly-convergent intra-element multigrid techniques [16,17]; for the Stokes operator of (36) we employ splitting schemes [11,12] or preconditioned Uzawa methods [4,14] to reduce the procedure to elliptic sub-problems. The key to minimal work per iteration is the use of tensor product elements, spaces, bases, and (consistent) quadratures, allowing for sum-factorization and efficient

matrix-vector product evaluations.

We note that the solution of (31) is stable for all time steps  $\Delta t$  ( $Q \leq 6$ ). However, in order to evaluate  $\phi$  from previous timesteps at the foot of the relevant characteristics, we need to solve a pure convection problem for  $\phi$  and  $\underline{u}$ . The details of this evaluation are given in (33), in which we have chosen to use an explicit third-order Adams-Bashforth integration scheme; the associated spectral element Courant condition is  $\Delta t_{cr} < \mathcal{O}(1/K^{1/d}N^2)$  [15]. It is important to note that our approach to solving the invariance equation (16) preserves the underlying tensor-product structure of the spatial discretization, and hence no costly re-interpolation is necessary. Indeed, if referencing were done only to the base geometry  $\underline{X}^{l,*}$ , interpolation would require  $\mathcal{O}(KN^{2d})$  operations, compared to  $\mathcal{O}(KN^{d+1})$  for our tensor-product scheme [34].

## 5.2 One-dimensional results for a passive scalar

In this section we consider the solution of the convection-diffusion equation (4) in one space dimension. In the first test problem we choose  $\Omega = ]0, 1[$ ,  $\nu = 0.01$ ,  $u = 1$ , with  $\phi(x, t = 0) = \sin(2\pi x)$ , and periodic boundary conditions. The exact solution is given by  $\phi(x, t) = e^{-\nu(2\pi)^2 t} \sin(2\pi(x - ut))$ . First, we demonstrate the temporal accuracy of the new Lagrangian-decoupling method. Figure 1 shows the  $L^\infty$ -error at a fixed time  $t = 2$  as a function of the time step  $\Delta t$  for a fixed spatial discretization  $K = 2$  and  $N = 15$ ; this spatial discretization assures that the temporal error is always dominating. The results clearly demonstrate that the temporal error is  $\mathcal{O}((\Delta t)^Q)$ , where  $Q$  is the order of the backward differentiation formula in (31). Since  $\Delta s$  is typically much smaller than  $\Delta t$ , the temporal error resulting from solving (33) will, in general, be much smaller than the temporal error resulting from solving (31), at least for  $Q \leq 3$ . We note that for pure convection ( $\nu = 0$ ), the only temporal error is due to the integration of the invariance equation (32)-(34); for this smooth problem, the accuracy *improves* as  $\nu$  decreases (in contrast to “mesh-upwinding”). Next, we demonstrate the spatial error of the scheme. In

Figure 2 we plot the  $L^\infty$ -error at a fixed time  $t = 2$  as a function of the polynomial degree  $N$ , for fixed  $K = 2$  elements, with  $Q = 3$ ,  $\Delta t = 0.01$ , and  $\Delta t/\Delta s = 100$ . As expected, we obtain exponential convergence as long as  $N \leq 10$ ; for  $N > 10$  the temporal error becomes dominating given our particular choice of  $Q$  and  $\Delta t$ .

As our second one-dimensional test problem we consider the steady state solution to (4) in  $\Omega = ]0, 1[$ ,  $\nu = 0.1$ ,  $u = 1$ , and essential boundary conditions  $\phi(x = 0, t) = 0$ ,  $\phi(x = 1, t) = 1$ . The exact solution as  $t \rightarrow \infty$  is given by  $\phi = \frac{e^{x/\nu} - 1}{e/\nu - 1}$ , which has a boundary layer of thickness  $\nu$  at  $x = 1$ . The numerical steady solution is obtained by integrating the unsteady convection-diffusion equation to a time  $t = 10$ , starting from an initial condition  $\phi(x, t = 0) = x$ . Figure 3 shows the  $L^\infty$ -error as a function of the time step  $\Delta t$  for  $Q = 1, 2, 3, 4$ , for a fixed spatial discretization  $K = 2$  and  $N = 11$ . Note that in this case the time step  $\Delta t$  has to be smaller than  $\mathcal{O}(\nu)$  before the expected convergence rate is observed. Also note that, unlike the standard Eulerian convection scheme, in which the steady state error is purely spatial, the error in our new scheme is contaminated by the temporal discretization due to the transformation of space into time. In Figure 4 we plot the  $L^\infty$ -error as a function of the polynomial degree  $N$  for fixed  $K = 2$ ,  $Q = 3$ ,  $\Delta t = 10^{-3}$ , and  $\Delta t/\Delta s = 10$ . The results demonstrate exponential convergence, at least for  $N < 10$ ; for  $N > 10$  the temporal error again becomes dominating.

We note that it is a drawback to the current method that  $\Delta t$  must be the same at all points on the domain, as this does not allow for local refinement near important spatial structures. Fortunately, the flow “through the wall” ( $u_m \hat{n}_m \neq 0$ ) associated with the normal boundary layer of Fig. 3 is not typical; if  $u_m \hat{n}_m = 0$ , the characteristics scheme is, in some sense, self-adaptive, as  $\Delta x \propto \int u dt'$ .

### 5.3 Two-dimensional results for a passive scalar

The first two-dimensional test problem we consider is pure convection ( $\nu = 0$ ) of a passive scalar  $\phi$  in  $\Omega = ]0, 1[^2$ . The boundary conditions are periodic conditions at

$x_1 = 0$  and  $x_1 = 1$ , and homogeneous Neumann conditions at  $x_2 = 0$  and  $x_2 = 1$ . The prescribed solenoidal velocity field is  $u_1 = 1$ ,  $u_2 = 0$ , and the exact solution is given by  $\phi(x_1, x_2, t) = \sin(2\pi(x_1 - u_1 t))\cos(2\pi x_2)$ . In Figure 5 we plot the error in the  $H^1$  semi-norm at a fixed time  $t = 5$  as a function of the polynomial degree  $N$  for fixed  $K = 4$  spectral elements,  $Q = 1$  and  $\Delta t = 0.1$ . The results clearly demonstrates that exponential convergence is achieved due to the smooth nature of the solution. Note that for this pure convection problem (for which our new scheme is not of practical interest, as  $\mathcal{W}_{\Delta t, s}^{inv}$  is effectively zero), the only temporal error is the error due to integrating the invariance equation (32), and thus  $Q = 1$ ,  $\Delta t = .1$  is sufficient. The sub timestep  $\Delta s$  is sufficiently small here that the spatial error is dominating.

As the second test problem we consider the steady state solution to the convection-diffusion equation (4) in the two-dimensional domain  $\Omega : x_1 \in ] - 1/2, 1/2[, x_2 \in ]0, 1[$ . The given velocity field is the stagnation potential-flow  $u_1 = x_1$ ,  $u_2 = -x_2$ . With boundary conditions  $\phi(x_1, x_2 = 0, t) = 1$  and  $\phi(x_1, x_2 = 1, t) = 0$  the steady state solution depends only on  $x_2$ , and is given as  $\phi = 1 - \frac{\int_0^{x_2} e^{-\xi^2/2\nu} d\xi}{\int_0^1 e^{-\xi^2/2\nu} d\xi}$ . In Figure 6 we plot the error in the  $H^1$  semi-norm at a fixed (effectively infinite) time  $t = 5$  as a function of the time step  $\Delta t$  for  $Q = 1, 2, 3$  for a fixed spatial discretization consisting of  $K = 4$  spectral elements of polynomial degree  $N = 10$ . Note that we impose the exact solution as essential boundary conditions on the whole domain boundary. The expected convergence rate  $\mathcal{O}((\Delta t)^Q)$  is clearly demonstrated. For  $Q = 1$  we repeat the experiment, but now imposing essential boundary conditions only along  $x_2 = 0$  and  $x_2 = 1$ , with homogeneous natural (Neumann) boundary conditions imposed along  $x_1 = -1/2$  and  $x_1 = 1/2$ ; the results demonstrate that the scheme works equally well for outflow boundary conditions. In Figure 7 we plot the error in the semi-norm at a fixed time  $t = 5$  as a function of the polynomial degree  $N$  for fixed  $K = 4$ ,  $Q = 2$  or  $3$ ,  $\Delta t = 10^{-3}$ , and  $5 \leq \Delta t/\Delta s \leq 10$ . Again, the results verify the spectral accuracy of the scheme.

Our stagnation flow results are different from the one-dimensional normal boundary

layer in two aspects. First, the boundary layer scale only as  $\nu^{1/2}$  here, as opposed to the atypical  $\nu$  for normal layers. Second, and more importantly, we note that there is no evidence in Fig. 6 of a boundary layer threshold effect in  $\Delta t$ , as  $u_m \hat{n}_m = 0$  and the effective  $\Delta x$  near the wall is therefore small. In most real viscous flows, in which no-slip is applied,  $u_2$  would in fact vary as  $-x_2^2$ , yielding even better accuracy than the slip  $u_2 = -x_2$  case studied here.

#### 5.4 Two-dimensional Navier-Stokes results

We now return to the unsteady Navier-Stokes system, which was the original motivation for the new scheme due to the potential savings in computational cost. As a test problem we consider flow in a  $x_1$ -periodic grooved channel, in which the flow is driven by a constant pressure gradient in the  $x_1$ -direction. These first results are intended only to demonstrate the stability of the method, and to hint at the potential computational savings possible.

The tests described below correspond to the geometry shown in Fig. 8a for a Reynolds number  $R = \frac{\bar{f}H^3}{\nu} = 25$ , where  $\bar{f}$  is the constant force (pressure gradient normalized by density), and  $H$  is the half-channel width. Only steady state results are presented. In all cases the spectral element mesh ( $X^{ls}$ ) is based on the  $K = 6$  elements shown in Fig. 8a, with  $N = 6$  in each element. In order to determine the accuracy and efficiency of the characteristic-decoupling scheme we first solve the problem by using a standard semi-implicit ‘‘Eulerian’’ scheme of the type (2), in which the convective term is treated with a third-order Adams-Bashforth scheme. A steady-state solution ( $t = 4$ ) is reached after 834 timesteps, with the solution shown in Figures 8b and 8c. The maximum velocity, normalized by  $H^2\bar{f}/\nu$ , is found to be  $U_{max} = 1.0$ .

Next, we repeat this test using the new Lagrangian-decoupling method. We use the first order  $Q = 1$  scheme (only steady-state results are examined), with a timestep  $\Delta t$  which is 50 times larger than that for the Eulerian scheme (note that for the Eulerian

scheme the Navier-Stokes timestep  $\Delta t$  is chosen from stability considerations,  $\Delta t = \Delta t_{cr}$ ; for the characteristic scheme only  $\Delta s$  in (33) is limited by  $\Delta t_{cr}$ ). The final time  $t = 4$  is now reached in 16 timesteps, giving the results shown in Figures 9a and 9b; in terms of computational cost, the new scheme obtained the  $t = 4$  solution 16 times faster than the standard approach. As regards accuracy, the two solutions look qualitatively the same, however, the maximum non-dimensional velocity in the characteristic case is  $U_{max} = 0.88$ , indicating a 10% error with respect to the Eulerian scheme. Although this discrepancy may appear to be due to the severe distortion of the mesh, shown in Fig. 9c as a plot of  $\underline{X}^{t; \Delta t / \Delta s}$ , tests on plane Poiseuille flow (in which *only* distortion effects are present) indicate that this degree of distortion is readily handled by the  $h = (K = 6, N = 6)$  approximation. Reduction of  $\Delta t$  or increasing  $Q$  reveals that the error is, in fact temporal; systematic numerical convergence results for Navier-Stokes are given in [25].

The results of these first Navier-Stokes calculations are by no means conclusive; tests to determine computational savings at fixed accuracy are currently underway [25]. Of particular importance is understanding the dependence of  $\Delta t'_{acc}$  and  $\mathcal{W}^{ch}$  on temporal order  $Q$ , the solution-induced deformation (in particular in boundary layers and near singularities), the spectral (or finite) element discretization, incomplete iteration, and the Stokes solver efficiency. It is clear, nevertheless, that the technique holds great promise in striking an efficient compromise between temporal stability and equation structure.

#### ACKNOWLEDGEMENTS:

This work was supported by the ONR and DARPA under Grant N00014-89-J-1610, by the ONR under Contract N00014-88-K-0188, by the NSF under Grant 8806925-ASC, and by NASA under NAS1-18605.

## References

- [1] F. Brezzi, On the existence, uniqueness and approximation of saddle point problems arising from Lagrangian multipliers, *R.A.I.R.O. Numer. Anal.* 8 (1974) 129-151.
- [2] M.O. Bristeau, R. Glowinski and J. Periaux, Numerical methods for the Navier-Stokes equations. Applications to the simulation of compressible and incompressible viscous flows, *Computer Physics Report*, to appear.
- [3] J. Cahouet and J.P. Chabard, Some fast three-dimensional finite element solvers for the generalized Stokes problem, *Int. J. Numer. Meth. in Fluids* 8 (1988) 869-895.
- [4] Y. Maday, D. Meiron, Patera, A.T. and Rønquist, E.M., Analysis of iterative methods for the steady and unsteady Stokes problem: Application to spectral element discretizations, *J. Comput. Phys.*, submitted.
- [5] A. Brooks and T.J.R. Hughes, Streamline upwind/Petrov Galerkin formulation for convection-dominated flows with particular emphasis on the incompressible Navier-Stokes equations, *Comp. Meth. Appl. Mech. Eng.* 32 (1982) 199.
- [6] C.W. Gear, *Numerical Initial Value Problems in Ordinary Differential Equations* (Prentice-Hall, Englewood Cliffs, 1971).
- [7] Y. Yamaguchi, C.J. Chang and R.A. Brown, Multiple buoyancy-driven flows in a vertical cylinder heated from below, *Phil. Trans. Roy. Soc. London A* (1984) 312-519.
- [8] A.J. Chorin, Numerical solution of incompressible flow problems, in: J.M. Ortega and W.C. Reinboldt, eds., *Studies in Numerical Analysis 2*, (SIAM, 1970) 64-71.
- [9] R. Temam, *Navier-Stokes Equations. Theory and Numerical Analysis* (North-Holland, Amsterdam, 1977).
- [10] S.A. Orszag and L.C. Kells, Transition to turbulence in plane Poiseuille flow and plane Couette flow, *J. Fluid Mech.* 96 (1980) 159.

- [11] K.Z. Korczak and A.T. Patera, An isoparametric spectral element method for solution of the Navier-Stokes equations in complex geometry, *J. Comput. Phys.* 62 (1986) 361-382.
- [12] P.F. Fischer, E.M. Rønquist and A.T. Patera, Parallel spectral element methods for viscous flows, in: *Proceedings of the Workshop on Methods and Algorithms for Partial Differential Equations on Advanced Processors, Austin, Texas, 1988, to appear.*
- [13] P.F. Fischer, Parallel spectral element methods for the incompressible Navier-Stokes equations (Ph.D. Thesis, Massachusetts Institute of Technology, 1989).
- [14] Y. Maday and A.T. Patera, Spectral element methods for the Navier-Stokes equations, in: A.K.Noor and J.T. Oden, eds., *State of the Art Surveys in Computational Mechanics* (ASME, New York, 1989) 71-144.
- [15] E.M. Rønquist, Optimal spectral element methods for the unsteady three-dimensional Navier-Stokes equations, (Ph.D. Thesis, Massachusetts Institute of Technology, 1988).
- [16] E.M. Rønquist and A.T. Patera, Spectral element multigrid. I. Formulation and numerical results, *J. Sci. Comput.* 2(4) (1987) 389-402.
- [17] Y. Maday and M. Munoz, Spectral element multigrid. II. Theoretical justification, *J. Sci. Comput.*, to appear.
- [18] O. Pironneau, On the transport-diffusion algorithm and its applications to the Navier-Stokes equations, *Numer. Math.* 38 (1982) 309-332.
- [19] B. Ramaswamy, Numerical simulation of unsteady viscous free surface flow, *J. Comput. Phys.*, submitted.
- [20] P. Gresho, S. Chan, R. Lee and C. Upson, A modified F.E.M. for solving the time-dependent incompressible Navier-Stokes equations, *Int. J. Num. Meth. Fl.* 4 (1984) 557-598 (Part 1) and 619-640 (Part 2).
- [21] P.J. Roache, *Computational Fluid Dynamics* (Hermosa Publishers, Albuquerque, 1982).

- [22] K. Kuwahara, Development of high-Reynolds-number-flow computations, in: K. Kuwahara, R. Mendez and S.A. Orszag, eds., *Lecture Notes in Engineering* 24 (Springer-Verlag, 1985) 28-40.
- [23] G. Strang and J. Fix, *An Analysis of the Finite Element Method* (Prentice-Hall, Englewood Cliffs, 1973).
- [24] C. Canuto, M. Hussaini, A. Quarteroni and T. Zang, *Spectral Methods in Fluid Dynamics* (Springer-Verlag, 1987).
- [25] Y. Maday, A.T. Patera and E.M. Rønquist, Analysis of a high-order Lagrangian-decoupling method for the incompressible Navier-Stokes equations, ICASE Report 89-53 (in preparation).
- [26] R.A. Adams, *Sobolev Spaces* (Academic Press, 1975).
- [27] L.W. Ho, A spectral element stress formulation of the Navier-Stokes equations (Ph.D. Thesis, Massachusetts Institute of Technology, 1989).
- [28] R. Glowinski, G. Golub, G. Meurant and J. Periaux, J., eds., *Proceedings of the First International Conference on Domain Decomposition Methods for Partial Differential Equations* (SIAM, Philadelphia, 1988).
- [29] P.F. Fischer and A.T. Patera, Parallel spectral element solution of the Stokes problem, *J. Comput. Phys.*, to appear.
- [30] I. Babuska and M.R. Dorr, Error estimates for the combined h- and p-version of the finite element method, *Numer. Math.* 37 (1981) 257.
- [31] B.A. Szabo, Mesh design for the p-version of the finite element method, *Comp. Meth. in Appl. Math. Engr.* 55 (1986) 181-197.
- [32] A.T. Patera, A spectral element method for Fluid Dynamics: Laminar flow in a channel expansion, *J. Comput. Phys.* 54 (1984) 468-488.

- [33] Y. Maday and E.M. Rønquist, Optimal error analysis of spectral methods with emphasis on nonconstant coefficients and deformed geometries, in Proc. Int. Conf. on Spectral and High-Order Meth. for Partial Differential Equations, Italy, June 1989, to appear.
- [34] S.A. Orszag, Spectral methods for problems in complex geometries, *J. Comput. Phys.*, 37 (1980) 37-70.
- [35] V. Girault and P.A. Raviart, P.A., Finite Element Approximation of the Navier-Stokes Equations (Springer-Verlag, Berlin, 1986).
- [36] Y. Maday, A.T. Patera and E.M. Rønquist, A well-posed optimal spectral element approximation for the Stokes problem, *SIAM J. Numer. Anal.*, to appear.
- [37] C. Bernardi, Y. Maday and A.T. Patera, A new non-conforming approach to domain decomposition: the mortar element method, in: H. Brezis and J.L. Lions, eds., *Nonlinear Partial Differential Equations and their Applications*, to appear.
- [38] Y. Maday, C. Mavriplis and A.T. Patera, Non-conforming mortar element methods: application to spectral discretizations, in: T. Chan, ed., *Proceedings of the 7th International Conference on Domain Decomposition Techniques for Partial Differential Equations* (SIAM, Philadelphia, 1988).
- [39] P.J. Davis and P. Rabonowitz, *Methods of Numerical Integration* (Academic Press, 1985).

## Figure Captions

**Figure 1.** A plot of the discretization error  $\| \phi - \phi_h \|_{L^\infty}$  at a fixed time  $t = 2$  as a function of the timestep  $\Delta t$  for a fixed (accurate) spatial discretization, when solving the convection-diffusion equation (4) using the new Lagrangian-decoupling method. The exact solution is given as  $\phi(x, t) = e^{-\nu(2\pi)^2 t} \sin(2\pi(x - ut))$  in the (periodic) domain  $\bar{\Omega} = [0, 1]$ , with  $\nu = 0.01$  and  $u = 1$ . The results show the (dominating) temporal error of the  $Q = 1$  ( $\circ$ ),  $Q = 2$  ( $\square$ ), and  $Q = 3$  ( $\triangle$ ) backward differentiation schemes.

**Figure 2.** A plot of the discretization error  $\| \phi - \phi_h \|_{L^\infty}$  at a fixed time  $t = 2$  as a function of the polynomial degree  $N$  in the  $K = 2$  fixed elements, when solving the convection-diffusion equation (4) using the new Lagrangian-decoupling method. The timestep is set small to minimize temporal pollution. The exact one-dimensional periodic solution is given as  $\phi(x, t) = e^{-\nu(2\pi)^2 t} \sin(2\pi(x - ut))$  for  $x \in \bar{\Omega} = [0, 1]$ , with  $\nu = 0.01$  and  $u = 1$ . Spectral convergence is achieved for  $N < 10$ ; for  $N > 10$  the (fixed) temporal error becomes dominating.

**Figure 3.** A plot of the steady-state discretization error  $\| \phi - \phi_h \|_{L^\infty}$  as a function of the timestep  $\Delta t$  for a fixed (accurate) spatial discretization, when solving the convection-diffusion equation (4) using the new Lagrangian-decoupling method. The exact one-dimensional steady-state boundary layer solution is given by  $\phi = \frac{e^{-x/\nu} - 1}{e^{-1/\nu} - 1}$  for  $x \in \bar{\Omega} = [0, 1]$  ( $\nu = 0.1$ ). The results show the (dominating) temporal error of the  $Q = 1$  ( $\circ$ ),  $Q = 2$  ( $\bullet$ ),  $Q = 3$  ( $\triangle$ ), and  $Q = 4$  ( $\Delta$ ) backward differentiation schemes.

**Figure 4.** A plot of the steady-state discretization error  $\| \phi - \phi_h \|_{L^\infty}$  as a function of the polynomial degree  $N$  in  $K = 2$  fixed elements, when solving the convection-diffusion equation (4) using the new Lagrangian-decoupling method. The timestep is set small to minimize temporal pollution. The exact one-dimensional steady-state boundary layer solution is given by  $\phi = \frac{e^{-x/\nu} - 1}{e^{-1/\nu} - 1}$  for  $x \in \bar{\Omega} = [0, 1]$  ( $\nu = 0.1$ ). Spectral convergence is achieved for  $N < 10$ ; for  $N > 10$  the (fixed) temporal error becomes dominating.

**Figure 5.** A plot of the discretization error in the  $H^1$  semi-norm,  $|\phi - \phi_h|_1$ , at a fixed time  $t = 5$  as a function of the polynomial degree  $N$  in  $K = 4$  fixed elements, when solving the convection equation (4) ( $\nu = 0$ ) using the new Lagrangian-decoupling method. The exact two-dimensional solution is given by  $\phi(x_1, x_2, t) = \sin(2\pi(x_1 - u_1 t))\cos(2\pi x_2)$  for  $(x_1, x_2) \in \bar{\Omega} = [0, 1]^2$ , with  $u_1 = 1, u_2 = 0$ . Periodic boundary conditions are imposed at  $x_1 = 0$  and  $x_1 = 1$ , with homogeneous Neumann conditions imposed at  $x_2 = 0$  and  $x_2 = 1$ . Spectral accuracy is achieved.

**Figure 6.** A plot of the steady-state discretization error in the  $H^1$  semi-norm,  $|\phi - \phi_h|_1$ , as a function of the timestep  $\Delta t$  for a fixed (accurate) spatial discretization, when solving the two-dimensional convection-diffusion equation (4) using the new Lagrangian-decoupling method. The exact steady-state solution is given as  $\phi = 1 - \frac{\int_0^{x_2} e^{-\xi^2/2\nu} d\xi}{\int_0^1 e^{-\xi^2/2\nu} d\xi}$  for  $x_1 \in [-1/2, 1/2], x_2 \in [0, 1]$ , for an imposed stagnation flow  $u_1 = x_1, u_2 = -x_2$ . With imposed Dirichlet boundary conditions for  $\phi$ , the results show the (dominating) temporal error for backward differentiation schemes of order  $Q = 1$  ( $\circ$ ),  $Q = 2$  ( $\square$ ), and  $Q = 3$  ( $\triangle$ ). For comparison we also plot the error for the case  $Q = 1$  with homogeneous Neumann conditions imposed along  $x_1 = \pm 1/2$  (outflow) ( $\bullet$ ).

**Figure 7.** A plot of the steady-state discretization error in the  $H^1$  semi-norm,  $|\phi - \phi_h|_1$ , as a function of the polynomial degree  $N$  in  $K = 4$  fixed spectral elements, when solving the two-dimensional convection-diffusion equation (4) using the new Lagrangian-decoupling method. The timestep is set small to minimize temporal pollution. The exact solution is given by  $\phi = 1 - \frac{\int_0^{x_2} e^{-\xi^2/2\nu} d\xi}{\int_0^1 e^{-\xi^2/2\nu} d\xi}$  for  $x_1 \in [-1/2, 1/2], x_2 \in [0, 1]$ , for an imposed stagnation flow  $u_1 = x_1, u_2 = -x_2$ . Spectral accuracy is achieved.

**Figure 8.** Two-dimensional Navier-Stokes solution in a  $x_1$ -periodic grooved channel at a Reynolds number  $R = \frac{UH^2}{\nu} = 25$ , in which the flow is driven by a constant pressure gradient in the  $x_1$  direction. Starting from rest, an approximately steady state solution is reached at a time  $t = 4$ . Here the numerical solution is obtained using a standard

(Eulerian) semi-implicit scheme described by equation (2), based on the spectral element mesh shown in Fig. 8a. In Fig. 8b and 8c we plot the solution in terms of streamlines and velocity vectors, respectively.

**Figure 9.** Two-dimensional Navier-Stokes solution in a  $x_1$ -periodic grooved channel at a Reynolds number  $R = \frac{\bar{L}H^2}{\nu^2} = 25$ , in which the flow is driven by a constant pressure gradient in the  $x_1$  direction. Starting from rest, an approximately steady state solution is reached at a time  $t = 4$ . Here the numerical solution is obtained using the new Lagrangian-decoupling method. In Fig. 9b and 9c we plot the solution in terms of streamlines and velocity vectors, respectively, and in Fig. 9c we indicate the mesh distortion that occurs in the invariance-equation integration. Note that although the characteristic method allows for large  $\Delta t$ , and hence rapid convergence to the steady-state, the method does not reduce the parametric stiffness associated with long timescales as  $R \rightarrow \infty$ .

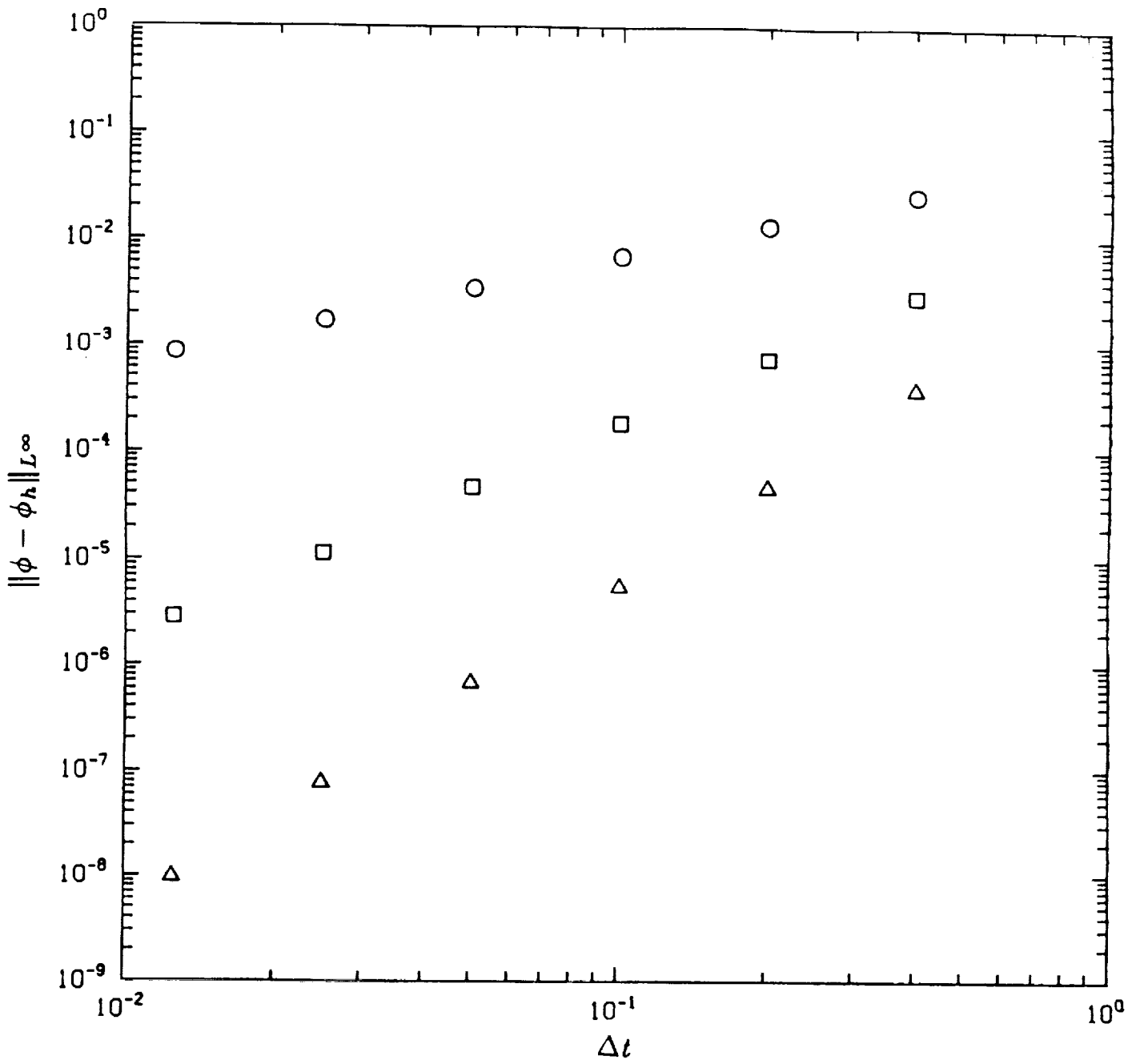


FIGURE 1

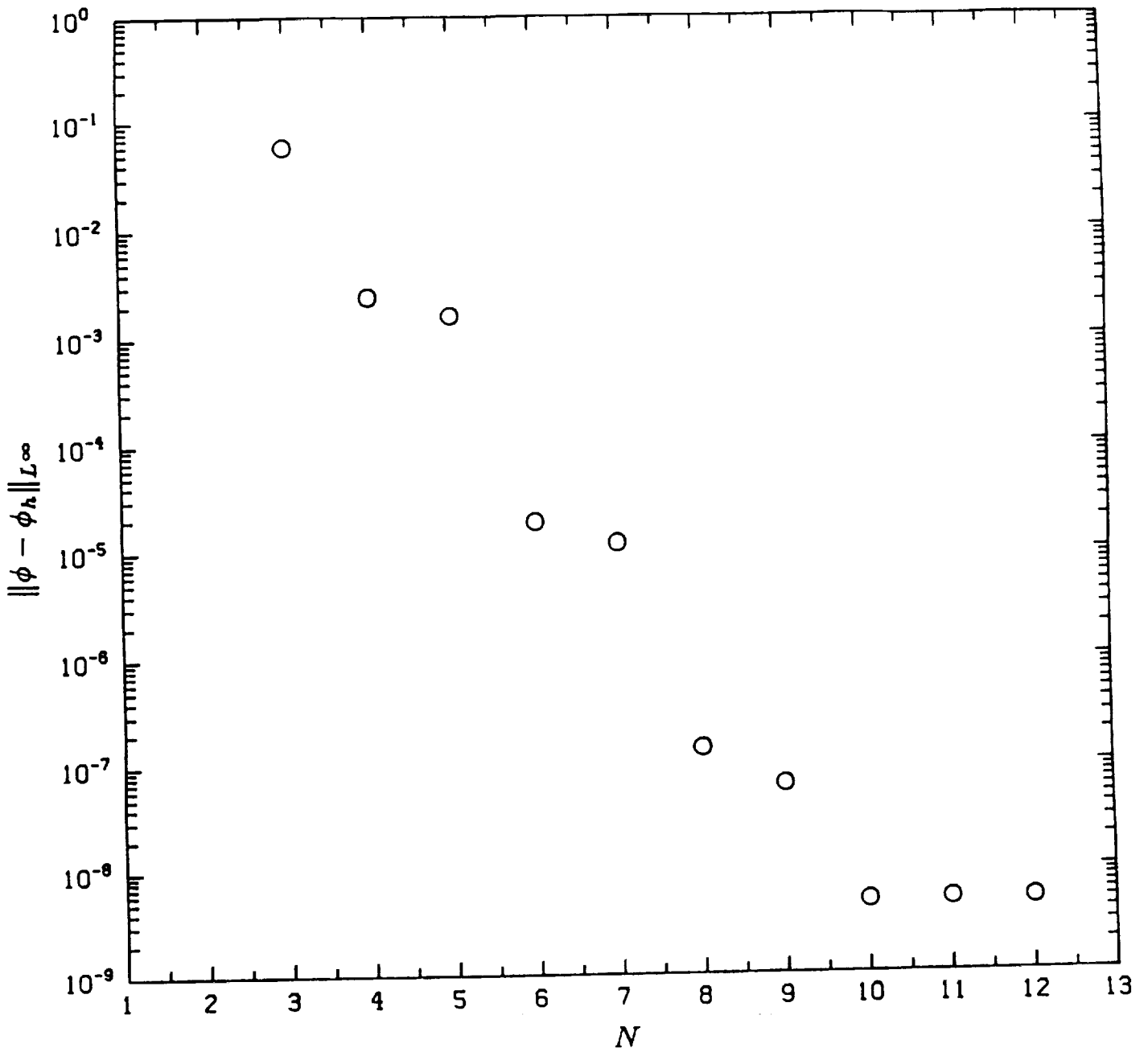


FIGURE 2

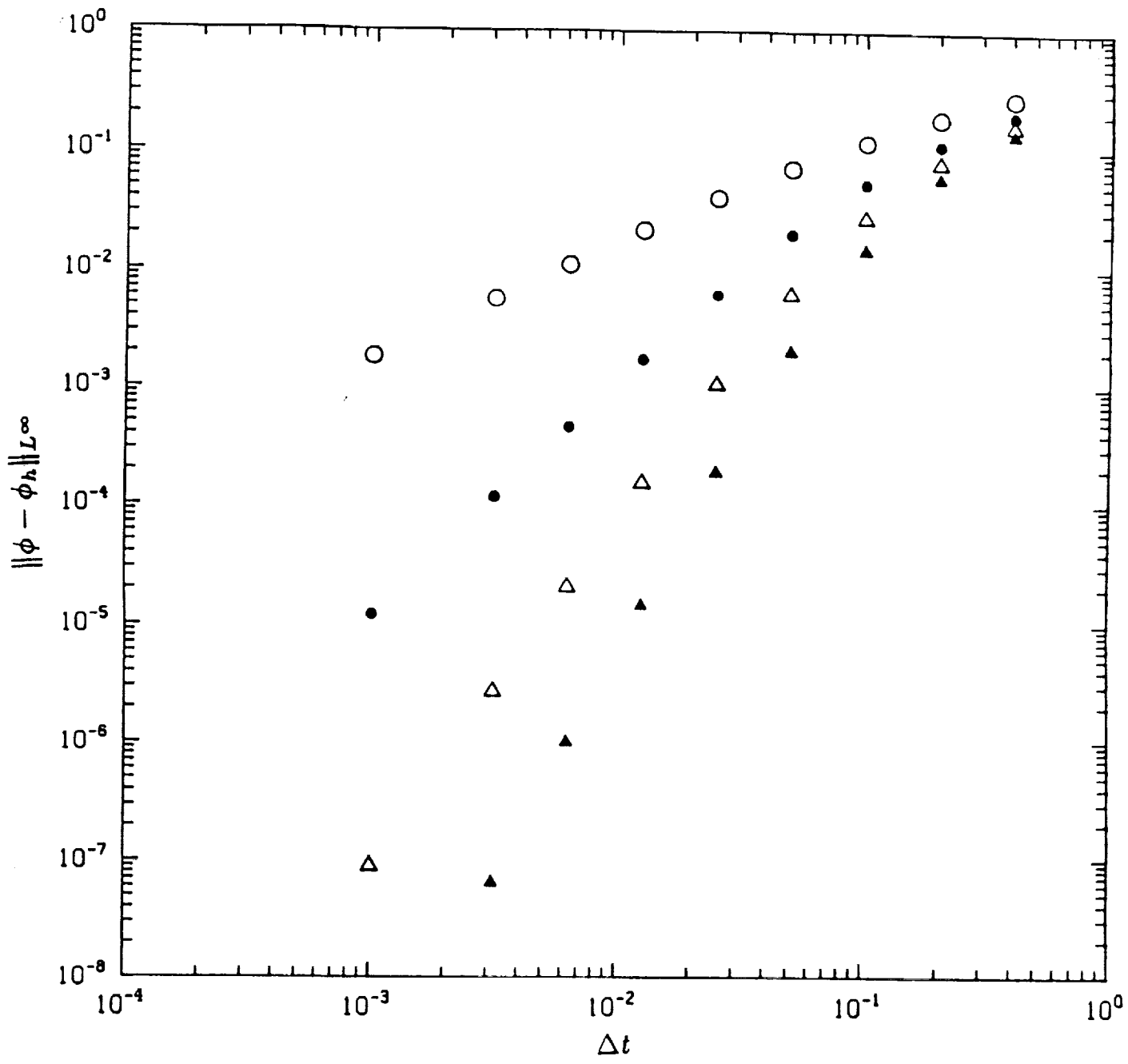


FIGURE 3

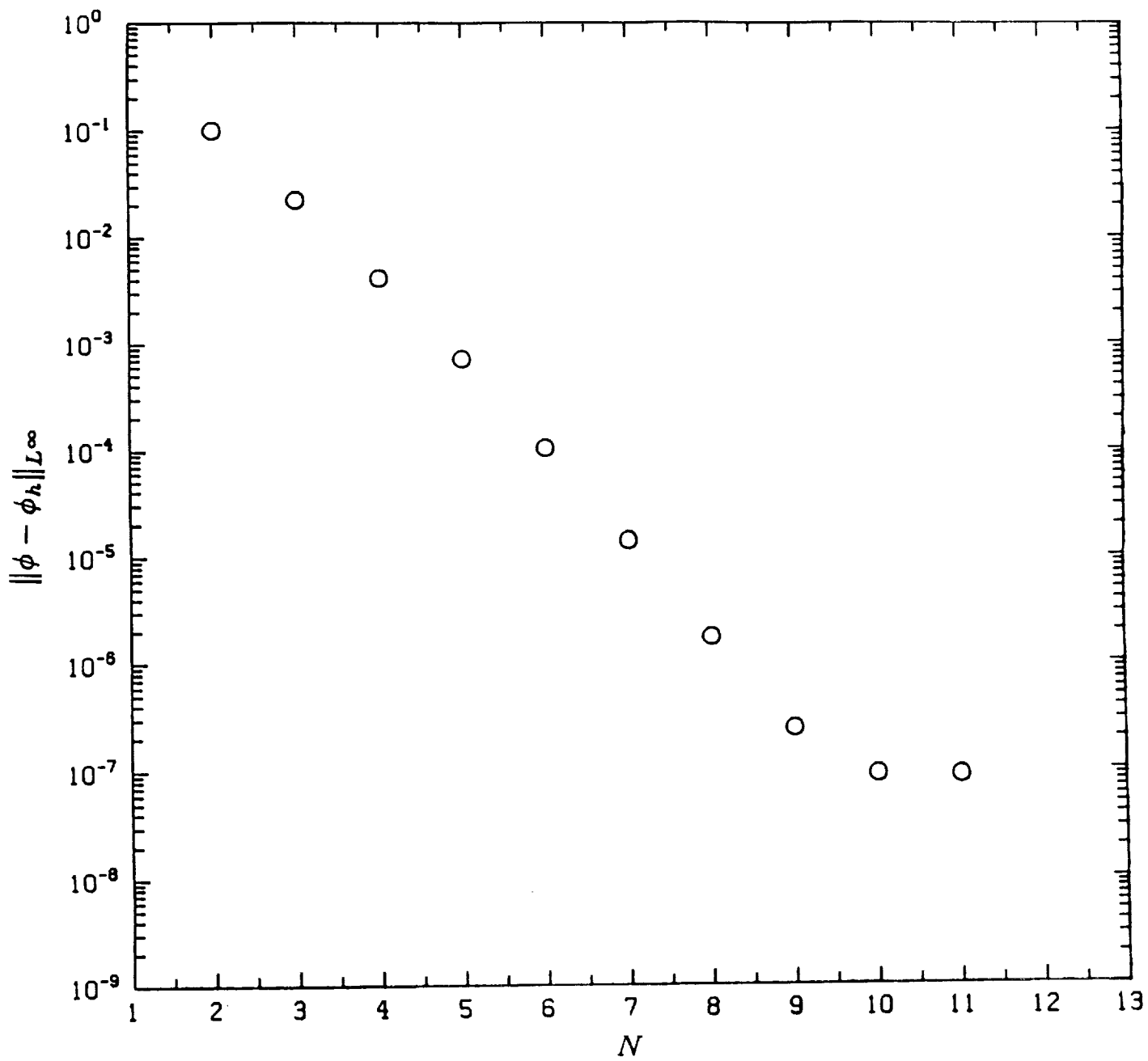


FIGURE 4

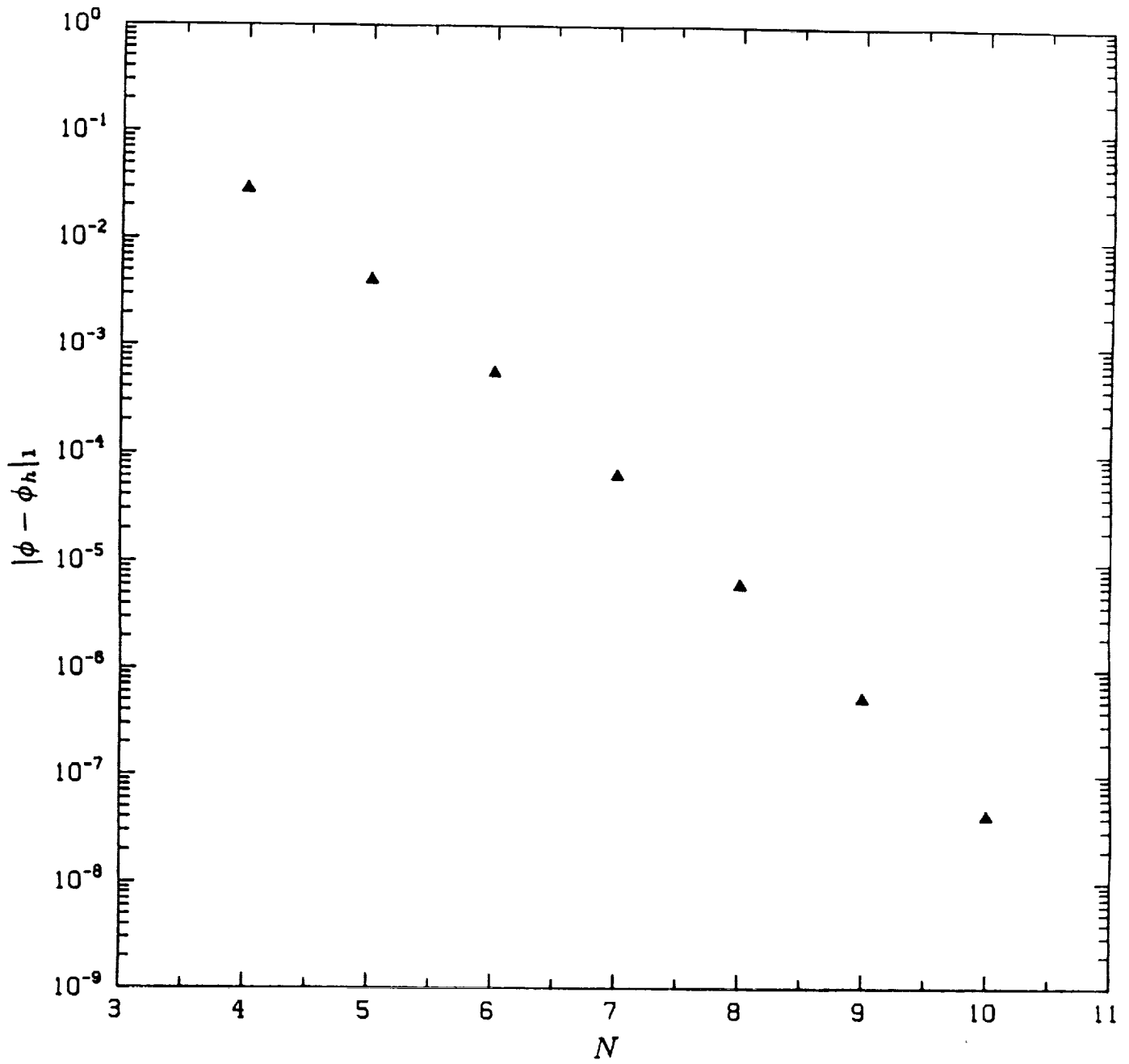


FIGURE 5

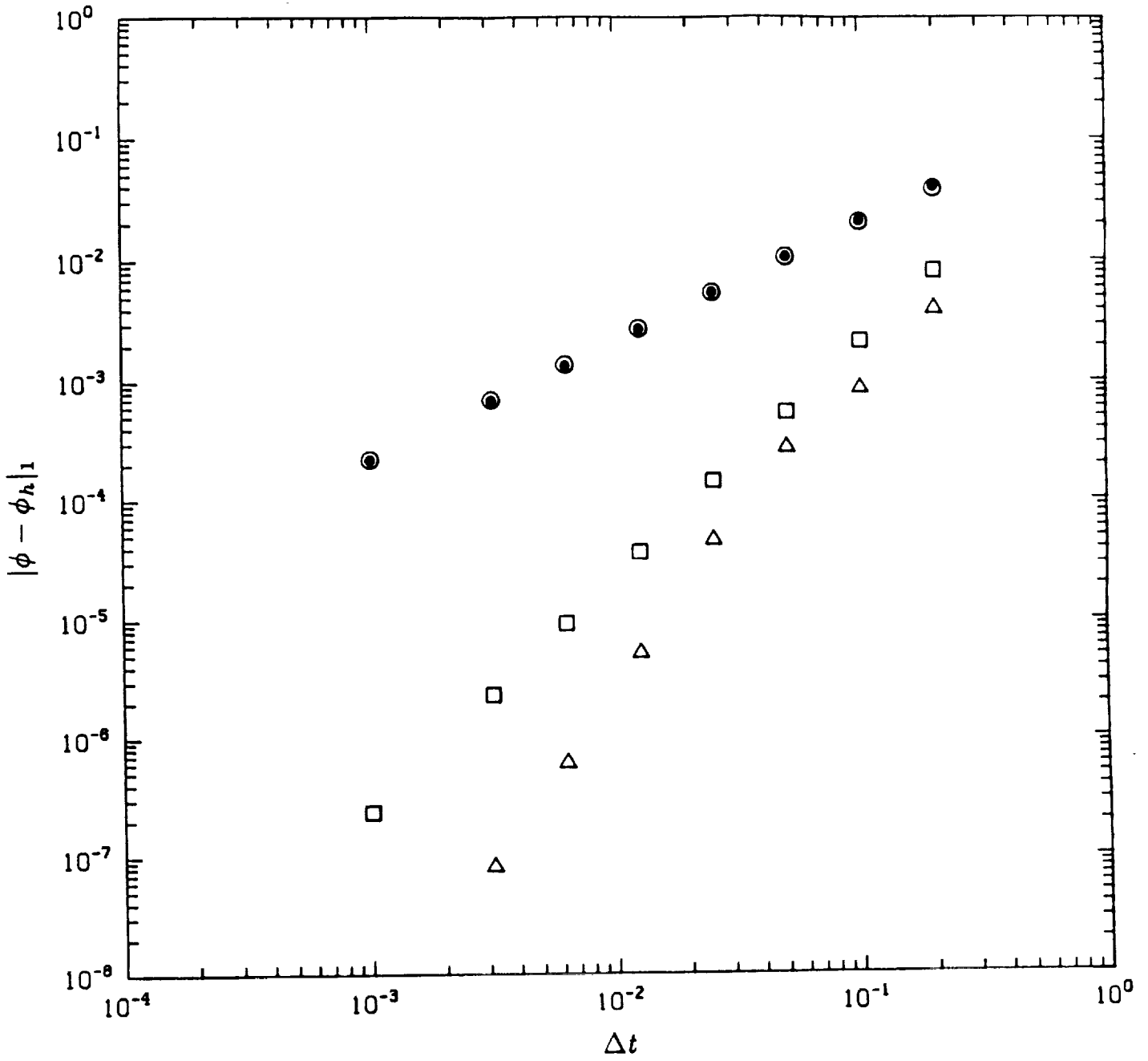


FIGURE 6

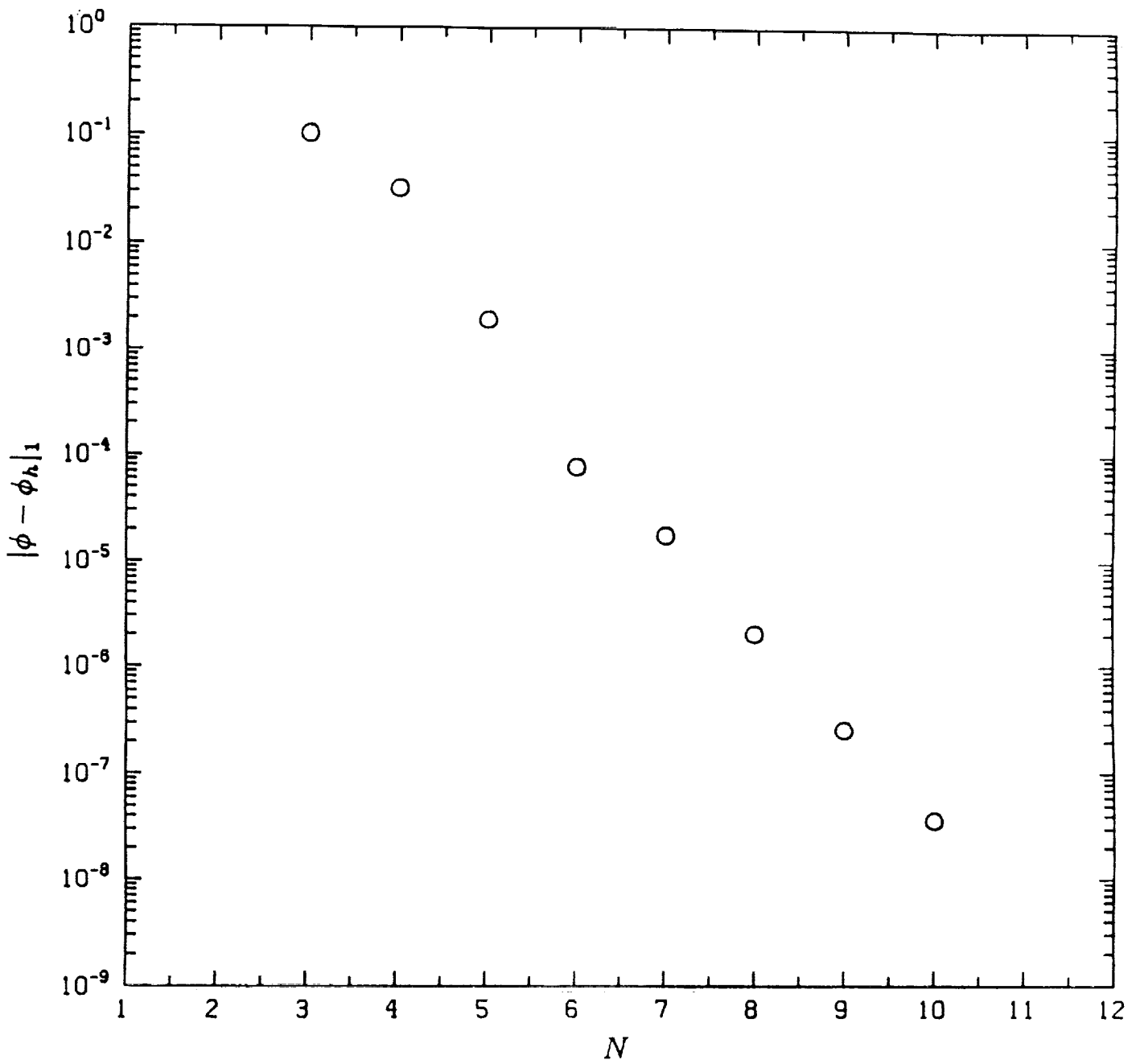


FIGURE 7

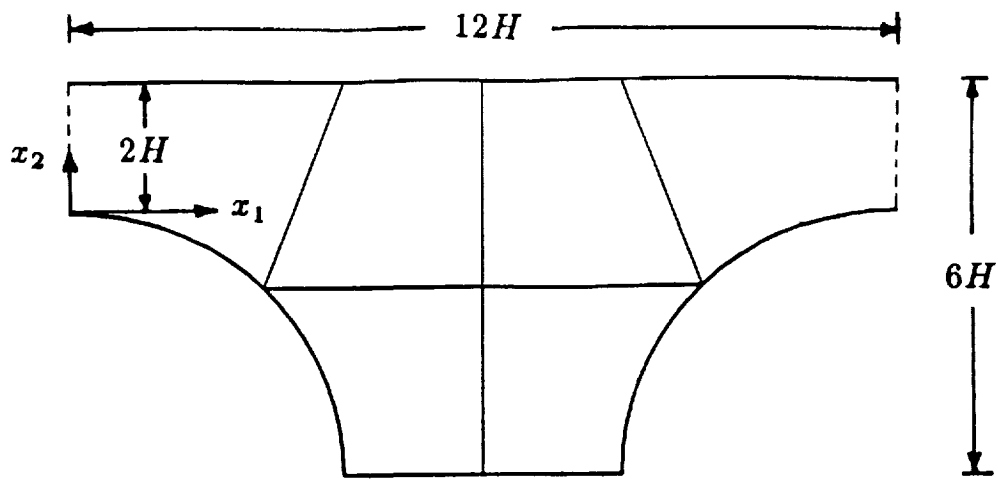


FIGURE 8 (a)

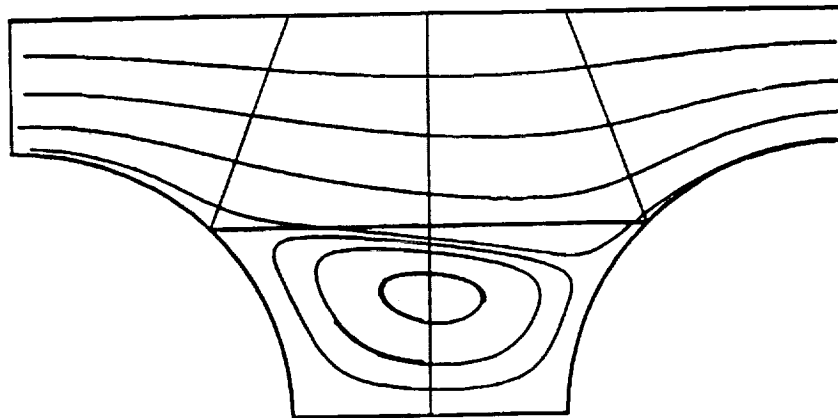


FIGURE 8 (b)

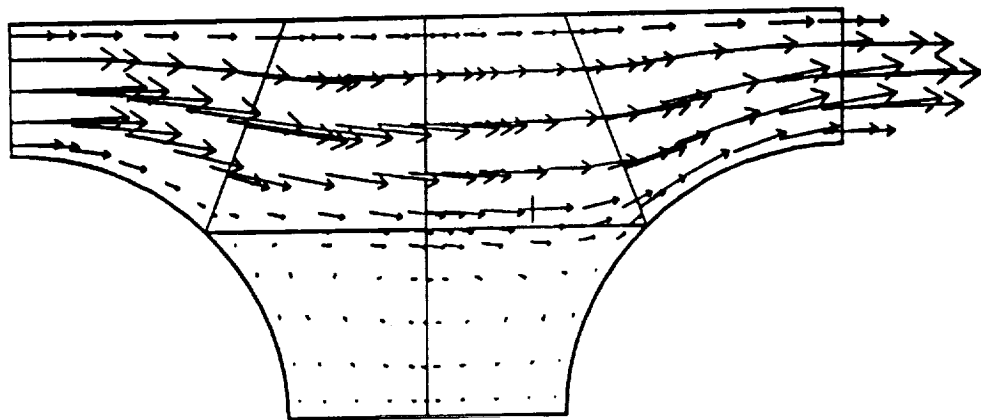


FIGURE 8 (c)

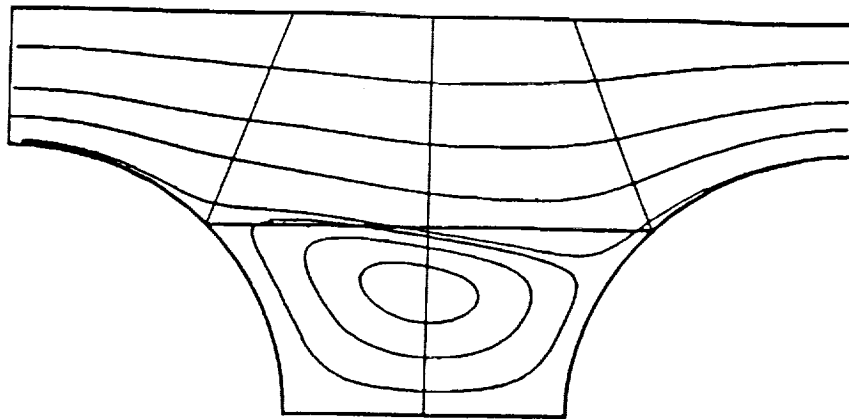


FIGURE 9 (a)

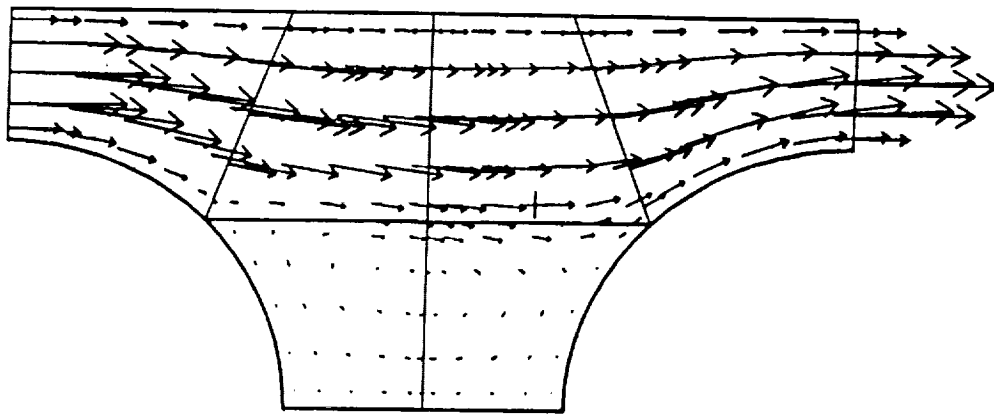


FIGURE 9 (b)

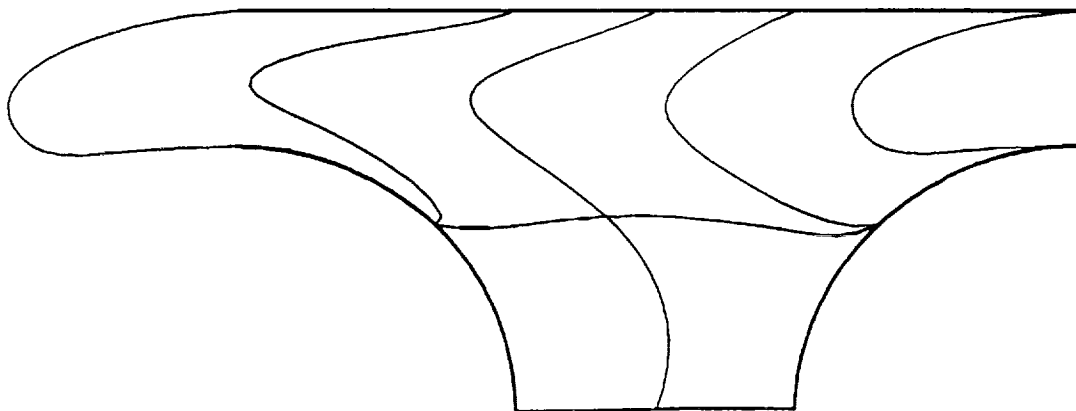


FIGURE 9 (c)



# Report Documentation Page

1. Report No. NASA CR-181903 ICASE Report No. 89-57		2. Government Accession No.		3. Recipient's Catalog No.	
4. Title and Subtitle  A HIGH-ORDER LAGRANGIAN-DECOUPLING METHOD FOR THE INCOMPRESSIBLE NAVIER-STOKES EQUATIONS				5. Report Date  September 1989	
				6. Performing Organization Code	
7. Author(s)  L. Ho, Y. Maday, A. Patera, E. Rönquist				8. Performing Organization Report No.  89-57	
				10. Work Unit No.  505-90-21-01	
9. Performing Organization Name and Address  Institute for Computer Applications in Science and Engineering Mail Stop 132C, NASA Langley Research Center Hampton, VA 23665-5225				11. Contract or Grant No.  NAS1-18605	
				13. Type of Report and Period Covered  Contractor Report	
12. Sponsoring Agency Name and Address  National Aeronautics and Space Administration Langley Research Center Hampton, VA 23665-5225				14. Sponsoring Agency Code	
				15. Supplementary Notes  Langley Technical Monitor: Proceedings of ICOSAMOM Meeting 1989 Richard W. Barnwell	
Final Report					
16. Abstract  In this paper we present a high-order Lagrangian-decoupling method for the unsteady convection-diffusion and incompressible Navier-Stokes equations. The method is based upon: Lagrangian variational forms that reduce the convection-diffusion equation to a symmetric initial value problem; implicit high-order backward-differentiation finite-difference schemes for integration along characteristics; finite element or spectral element spatial discretizations; mesh-invariance procedures and high-order explicit time-stepping schemes for deducing function values at convected space-time points. The method improves upon previous finite element characteristic methods through the systematic and efficient extension to high order accuracy, and the introduction of a simple structure-preserving characteristic-foot calculation procedure which is readily implemented on modern architectures. The new method is significantly more efficient than explicit-convection schemes for the Navier-Stokes equations due to the decoupling of the convection and Stokes operators and the attendant increase in temporal stability. Numerous numerical examples are given for the convection-diffusion and Navier-Stokes equations for the particular case of a spectral element spatial discretization.					
17. Key Words (Suggested by Author(s))  characteristic, incompressible Navier-Stokes, spectral methods			18. Distribution Statement  64 - Numerical Analysis  Unclassified - Unlimited		
19. Security Classif. (of this report)  Unclassified		20. Security Classif. (of this page)  Unclassified		21. No. of pages  47	22. Price  A03

